- 1 Meteorological factors control landslide processes in a high-Arctic glacier basin (Ny-
- 2 Ålesund, Svalbard)
- 3 Journal: Geomorphology

- 5 Erik Kuschel<sup>1\*</sup>, Florian Tolle<sup>2</sup>, Vinzent Klaus<sup>3</sup>, Ursula Laa<sup>4</sup>, Alexander Prokop<sup>5,6</sup>, Jean-Michel
- 6 Friedt<sup>7</sup>, Eric Bernard<sup>2</sup>, & Christian Zangerl<sup>1</sup>

7

- 8 (1) University of Natural Resources and Life Sciences, Institute of Applied Geology, Vienna,
- 9 Austria
- 10 (2) Université de Franche-Comté, CNRS, ThéMA, F-25000 Besançon, France
- 11 (3) University of Natural Resources and Life Sciences, Institute of Meteorology and
- 12 Climatology, Vienna, Austria;
- 13 (4) University of Natural Resources and Life Sciences, Institute of Statistics, Vienna, Austria;
- 14 (5) Snow Scan GmbH, Vienna, Austria;
- 15 (6) University of Vienna, Department of Geodynamics and Sedimentology, Vienna, Austria;
- 16 (7) FEMTO-ST, Time & Frequency, 15 Avenue de Montboucon, 25000 Besançon, France;
- 17 (8) ThéMA, Université de Franche-Comté, CNRS, F-25000 Besançon, France
- 18 \*Corresponding Author: erik.kuschel@boku.ac.at

19

- 20 **Keywords:** Landslides, Paraglacial geomorphology, Remote Sensing, Terrestrial Laser
- 21 Scanning, Svalbard, Arctic, Climate Change

22

23

24

# **Abstract**

25

26

27

28

29

30

31

32

33

34

35

36

37

38

39

40

41

42

43

44

45

46

47

48

49

50

Landslide processes are one of the dominant agents of erosion and sediment transport on sediment-mantled slopes in arctic environments. Increased landslide activity is anticipated as climate change is projected to decrease mountain slope stability. High-Arctic environments serve as crucial observatories for investigating current and future landslide dynamics within a changing climate, particularly due to arctic amplification effects. Despite the significance of Arctic regions, empirical evidence regarding landslide processes in high latitudes is often lacking. This scarcity can be attributed to the absence of long-term, high-resolution terrain data with sufficient temporal resolution to assess the impact of meteorological boundary conditions on landslide dynamics altered by climate change. However, addressing this gap in empirical evidence is essential for understanding the complex interplay between meteorological variables and landslide evolution in Arctic environments. This study presents a unique high-resolution remote sensing dataset within a high-Arctic glacier basin acquired over a 10-year period. Through the combination of terrestrial laser-scanning and an autonomous camera network, we were able to investigate the impact of meteorological boundary conditions on the trigger mechanisms of landslides and unravel paraglacial slope evolution following recent glacier retreat on the example of the Austre Lovénbreen glacier basin (Svalbard, Norway). During the observation period, 171 distinct landslide events were identified. Translational debris slides accounted for approximately 96% of the total sediment flux observed, with debris flows acting as a secondary agent of sediment transport. The landslide activity significantly increased between 2011 and 2021. Heavy rainfall events primarily influence the frequency and magnitude of landslides during the hydrological summer, while the duration and intensity of the thawing period serve as the principal control for landslide initiation. In conclusion, this study highlights the significant impact of meteorological factors on landslide frequency and magnitude within high-Arctic glacier basins, shedding light on the dynamics of paraglacial slope modification in Arctic environments.

# 1. Introduction

51

52

53

54

55

56

57

58

59

60

61

62

63

64

65

66

67

68

69

70

71

72

73

74

Landslides are one of the most dominant erosion and sediment transport processes in mountainous terrain and often pose a significant risk to communities and infrastructure worldwide (Ballantyne, 2002; Gariano & Guzzetti, 2016; Zangerl et al., 2008). Climate change influences a wide range of processes (e.g. glacier retreat, permafrost thaw), which are projected to decrease the stability of mountain slopes (IPCC, 2014). From a theoretical view, there are clear indicators that climate change will lead to increased landslide activity (Crozier, 2010; Gariano & Guzzetti, 2016; Huggel et al., 2012; Seneviratne et al., 2012). However, empirical evidence is often lacking as meteorological boundary conditions altered by climate change may have different and often contrasting effects on landslide processes(Gariano & Guzzetti, 2016; IPCC, 2014). As the rate of measured global temperature change increases with latitude and elevation (Francis et al., 2017; Pepin et al., 2015), high-Arctic environments are an important observatory for investigating current and future landslide dynamics (Patton et al., 2019). Paraglacial slopes are constantly subjected to terrain changes by gravitational mass wasting processes (e.g. landslides, surface wash, snow avalanches) due to the rapid adjustment of recently deglaciated landscapes to nonglacial conditions (Ballantyne, 2002; Church & Ryder, 1972). The rapid readjustment of rock walls and drift-mantled slopes through landslide processes (e.g. rockfall, debris flows and debris slides) may lead to the formation of complex sediment-mantled slope systems, whose temporal and spatial evolution are influenced by lithological, glaciological, climatological and topographic conditions (Akerman, 1984; André, 1990, 1996; Ballantyne, 2002; Harris et al., 2009; Jahn, 1967; Mountains et al., 1976; Rapp, 1960)The results of these erosion and sedimentation processes can be seen in the vast areas

of reworked sediment draped over the slopes of Svalbard (De Haas et al., 2015).

Landslides are a mass of rock, debris or earth moving down a slope (Cruden, 1991), which develop in time through several stages (Terzaghi, 1950). Besides the material, landslide processes are structured into different movement types, such as falling, toppling, sliding, flowing, spreading and slope deformation (Hungr et al., 2014). This study focuses on the formation of different landslide types (e.g. translational debris slides, debris flows) and hence utilises the established landslide terminology developed by Cruden & Varnes (1996) and updated by Hungr et al., (2014).

Translational debris slides are characterised by the downslope movement of granular material on a planar surface, which may develop flow-like features after moving a specific travel distance (Hungr et al., 2014). Debris slides are often described as active layer detachments within permafrost literature and, therefore, related to the thermal impact of these slope-destabilizing phenomena (e.g. Ballantyne, 2002; French, 2013; Lewkowicz & Harris, 2005). In contrast, debris flows are rapid and long runout surging flows of water-saturated debris in established gullies or drainage channels, entraining material along their flow path, which may lead to the formation of debris fans and levees (Ballantyne, 2002; De Haas et al., 2015; Hungr et al., 2014).

The impact of landslides on paraglacial slopes is well documented by many authors and embedded in the paraglacial concept (Ballantyne, 2002; Church & Ryder, 1972). Numerous studies have investigated talus slope volumes to derive rock wall retreat rates (André, 1986; Berthling & Etzelmüller, 2007; Matsuoka, 1991; Rapp, 1960; Siewert et al., 2012). Others focus on the duration of paraglacial periods affecting the slopes (Mercier et al., 2009). The ongoing paraglacial response of sediment-mantled slopes through landslide processes has been assessed and mapped (Curry, 1999; De Haas et al., 2015; Mercier et al., 2009; Rapp, 1960; Tolgensbakk & Sollid., 1980). However, data on the impact of meteorological factors such as phases with strong rainfall and elevated temperature on the formation of distinct landslides in the surroundings of retreating glaciers are rare, especially for the high-Arctic

environment. The reason for this is the lack of long-term terrain data, with a spatiotemporal resolution high enough to detect slope processes reaching depths of only a few meters, as suggested by Patton et al. (2019). This study attempts to fill data gaps by applying multi-temporal terrestrial laser scanning on slopes of the Austre Lovénbreen glacier basin in Svalbard to investigate the formation characteristics and the temporal evolution of landslide processes under climate change. Thus, the objectives of this study comprise i) to provide multi-temporal high-resolution terrestrial laser scan data, ii) identification, characterisation, and quantification of landslide processes, and iii) investigating the preparatory and triggering factors for the spatiotemporal evolution of landslides within the Austre Lovénbreen Basin. Furthermore, we show that translational debris slides are the primary source of sediment transport on steep sediment-mantled slopes in a high-Arctic glacier valley and that meteorological factors significantly influence spatial and temporal development.

# 2. The Austre Lovénbreen glacier basin

The Austre Lovénbreen basin is dominated by the Austre Lovénbreen glacier, a small land-based polythermal glacier (Irvine-Fynn et al., 2011) with an elevation ranging from 50 to 550 m a.s.l. The glacier has shown a constant but irregular retreat since the Little Ice Age, and in 2013, it covered a surface area of 4.61 km², less than 43% of the total basin surface of approximately 10.45 km². In contrast, the glacier covered almost the entire proglacial area in the 1930s and about 50% of the basin in the 1980s (Hagen et al., 2003; Marlin et al., 2017). However, recent studies showed that significant amounts of glacier ice are located below the sediment-mantled slopes, yielding a 10% uncertainty on the glacier area (Bernard et al., 2014). The present-day glacier is constrained by alpine mountain peaks, such as Slåttofjellet (580 m a.s.l.), Haavimbfjellet (783 m a.s.l.), and Nobilefjellet (876 m a.s.l.) and the proglacial area in the north (Figure 1).

The slopes of the Austre Lovénbreen basin are composed of steep rock walls in the upper section and unconsolidated angular debris formed by paraglacial erosion processes in the lower section, which were glacially reworked in several areas. These loose slope sediments adjust to their natural slope angle, which ranges from 38 to 42°, and thus are highly susceptible to landslide processes, leading to ongoing morphological changes.

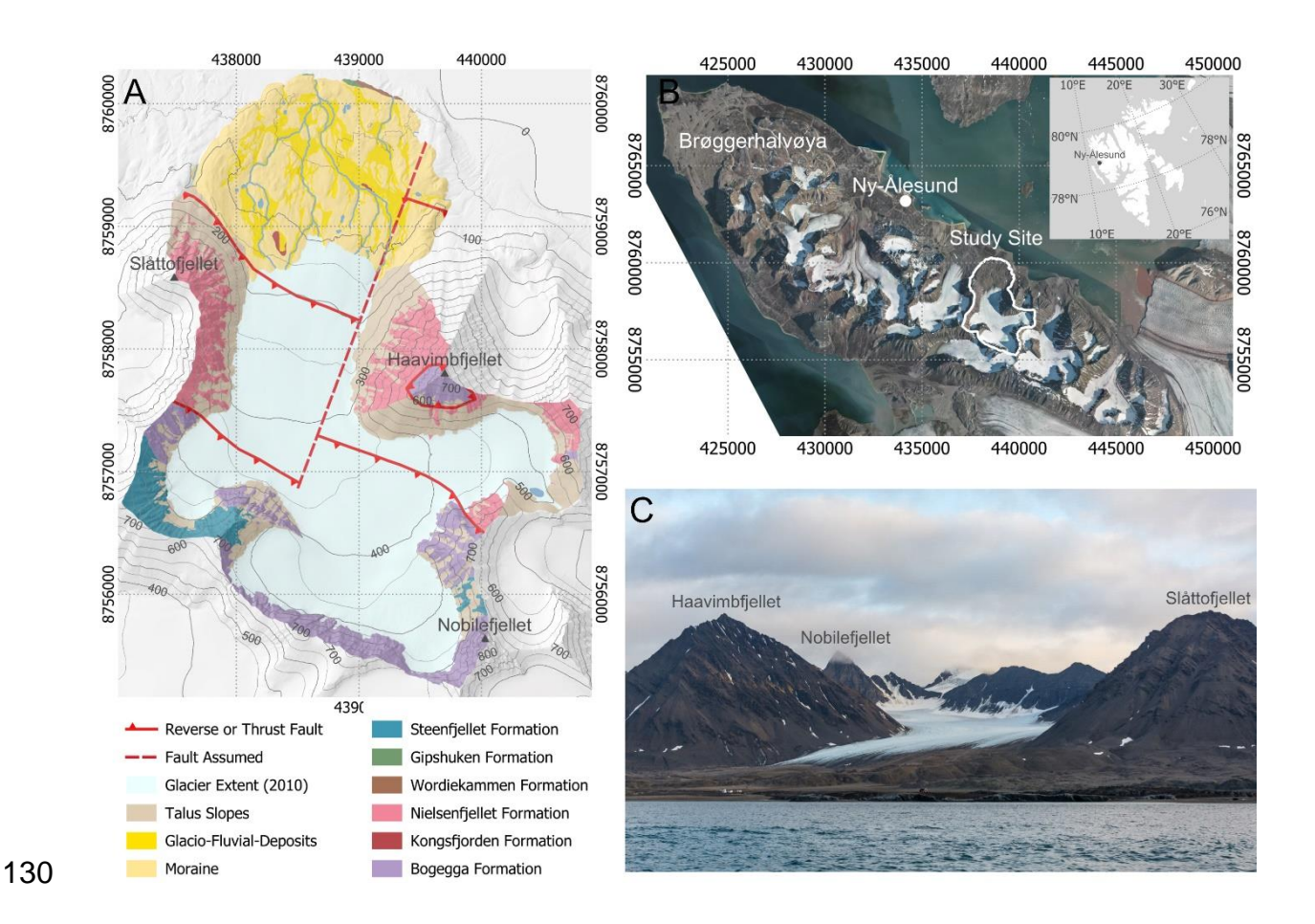


Figure 1: Geographical and geological setting of the Austre Lovénbreen study site. A) Geological map of the study site based on the field surveys; Lineations of structural features adopted from Hjelle et al. (1999); B) Overview map of the Brøggerhalvøya with Ny-Ålesund and the Study site; C) Extent of the Austre Lovénbreen glacier in 2017 as seen from NW, with surrounding mountain peaks.

Geologically, the Austre Lovénbreen basin is located in the Kongsvegen group, situated along the northernmost part of the Tertiary fold and thrust belt of western Spitsbergen, accompanied by several north-south striking faults and characterised by nine NE- to NNE-vergent thrust

sheets (Barbaroux, 1967; Bergh et al., 2000; Hjelle et al., 1999; Saalmann & Thiedig, 2001, 2002). The Kongsvegen group consist of low to medium metamorphic rocks, including mica schists interlayered with marble, quartzite or gneisses, having the highest metamorphic grade (Bogegga Formation), the greyish to yellowish dolomite marbles (Steenfjellet Formation) and phyllites with quartzite layers (Nielsenfjellet Formation) (Hjelle et al., 1999).

Located at 78°N, the study site is characterised by a high arctic maritime climate (Eckerstorfer & Christiansen, 2011). The North Atlantic current moderates the temperature at Svalbard compared to other regions at the same latitude (Maturilli et al., 2019), resulting in a mean annual air temperature (MAAT) of - 4 °C in Ny-Ålesund, 4 km from the Austre Lovénbreen glacier, between 1991 and 2020. The snow cover period typically extends from September or October until June. The average annual precipitation in Ny-Ålesund is around 470 mm, with a peak of monthly precipitation in autumn and winter. However, the amount of precipitation has been rising sharply in the last few years. The recent temperature increase due to global warming has been more pronounced around Svalbard than anywhere else on Earth (IPCC, 2021; Nordli et al., 2014). The MAAT in Ny-Ålesund increased from -5.7 °C between 1980 and 2000 to -3.6 °C between 2000 and 2020.

# 3. Material and Methods

# 3.1. Lidar data acquisition and processing

Terrestrial lidar data acquisition was performed annually from 2012 to 2018 and twice in 2021 using a Riegl LMS-420i (2012), a Riegl LPM-321 (2013-2015) and a Riegl VZ-6000 (since 2016) (RIEGL, 2010a, 2010b, 2016). TLS campaigns in 2019 and 2020 were impossible due to difficult pandemic restrictions. Two campaigns were conducted in 2021, capturing the prefailure (e.g., no observable landslides; 2021-1) and the post-failure state (2021-2). The technical upgrade of the utilised equipment has followed the overall improvement of available terrestrial lidar technology since 2012, increasing overall performance (e.g., range, beam

divergence, resolution, measurement speed) (Telling et al., 2017). The increased range of the Riegl VZ-6000, allowed the implementation of additional scan positions (e.g., Haavimbfjellet peak). Since 2016, monitoring almost the entire glacier basin (>95%) has been possible, whereas previous scans were only conducted in the context of individual slopes. Data gaps result from occlusions (e.g., crevasses, meltwater channels) and meltwater on the glacier surface (e.g., laser beam absorption) (Abellán et al., 2014; Prokop, 2008). Referenced colour images were acquired by the internal camera of the VZ-6000 or a calibrated high-resolution digital camera mounted on the respective laser scanners. The data acquisition was performed at the end of the ablation period and in sync with the measurement of the ablation stakes (Friedt et al., 2012) installed on the Austre Lovénbreen glacier.

More than 300 scans from 13 different scan positions were carried out, resulting in point cloud resolutions between approx. 0.05 m and 0.40 m within the study site (approx. 0.05 m to 0.20 m at the sediment-mantled slopes). Georeferencing, fine registration of individual laser scans and subsequent multi-temporal registration was done using an ICP algorithm implemented within the Riegl RiSCAN Pro software (Besl & McKay, 1992; Chen & Medioni, 1991; RIEGL, 2013). A reference point cloud, derived from an available 5x5 m Digital Elevation Model (DEM) in UTM coordinates (EPSG:25833), was used for geo-referencing the TLS data (MET Norway, 2021). The DEMs used in the further distance change analysis were derived for every TLS campaign from the registered and geo-referenced point clouds within CloudCompare with a resolution of 0.25x0.25 m (CloudCompare, 2021). Interpolation of the data was not performed to avoid the introduction of errors.

### 3.2. Mapping and volume calculation

Analyses of terrain changes were investigated through DEMs of Difference (DOD) created with the software Geomorphic Change Detection 7.4.1.0 (Wheaton et al., 2010) and diffuse hillshades created with the ambient occlusion method implemented in SAGA GIS (Tarini et

al., 2006). A spatially variable level of detection with a confidence interval of 95% (LOD95%) was calculated to differentiate between real changes and data noise (Fey & Wichmann, 2017; Lague et al., 2013; Prokop & Panholzer, 2009). Landslide processes (e.g., debris slides, debris flows) were mapped based on the DOD and hillshades and validated by field surveys. The results were used as Areas of Interest (AOI).

Several debris slides had their runout onto the glacier. Thus, it was not possible to quantify the accumulation zone as the exact elevation of the glacier surface during individual sliding events could not be determined. Therefore, the volume of each debris slide was investigated using AOI masks of the zone of depletion (Cruden & Varnes, 1996) to reduce uncertainties in the qualitative analysis and avoid quantifying the adjacent glacier ice volume changes.

# 3.3 Automated camera system monitoring and image analysis

A comprehensive investigation of causal relationships between meteorological conditions and the spatial and temporal occurrence of debris slides within the Austre Lovénbreen basin requires higher temporal resolution than annually performed TLS measurements. Therefore, a network of autonomous operating cameras (Figure 2) from the long-term observatory project monitoring the Austre Lovénbreen since 2007, providing a surface coverage of 96% of the glacier and the adjacent slopes (Bernard et al., 2013; Friedt et al., 2023). Thus, the date of failure, triggering mechanisms and temporal evolution of individual debris slides could be investigated, provided that visibility was not limited by poor weather. Furthermore, the identification, dating and quantification of landslides occurring in the years 2019 and 2020 was done by the available camera images. An additional TLS campaign in early 2021, before any seasonal landslide activity occurred, allowed to mitigate data gaps in the time-series of the annual landslide activity. Furthermore, the camera data allowed for a qualitative analysis of

landslide activity since 2007 within the Austre Lovénbreen basin, extending the observation period by five years.

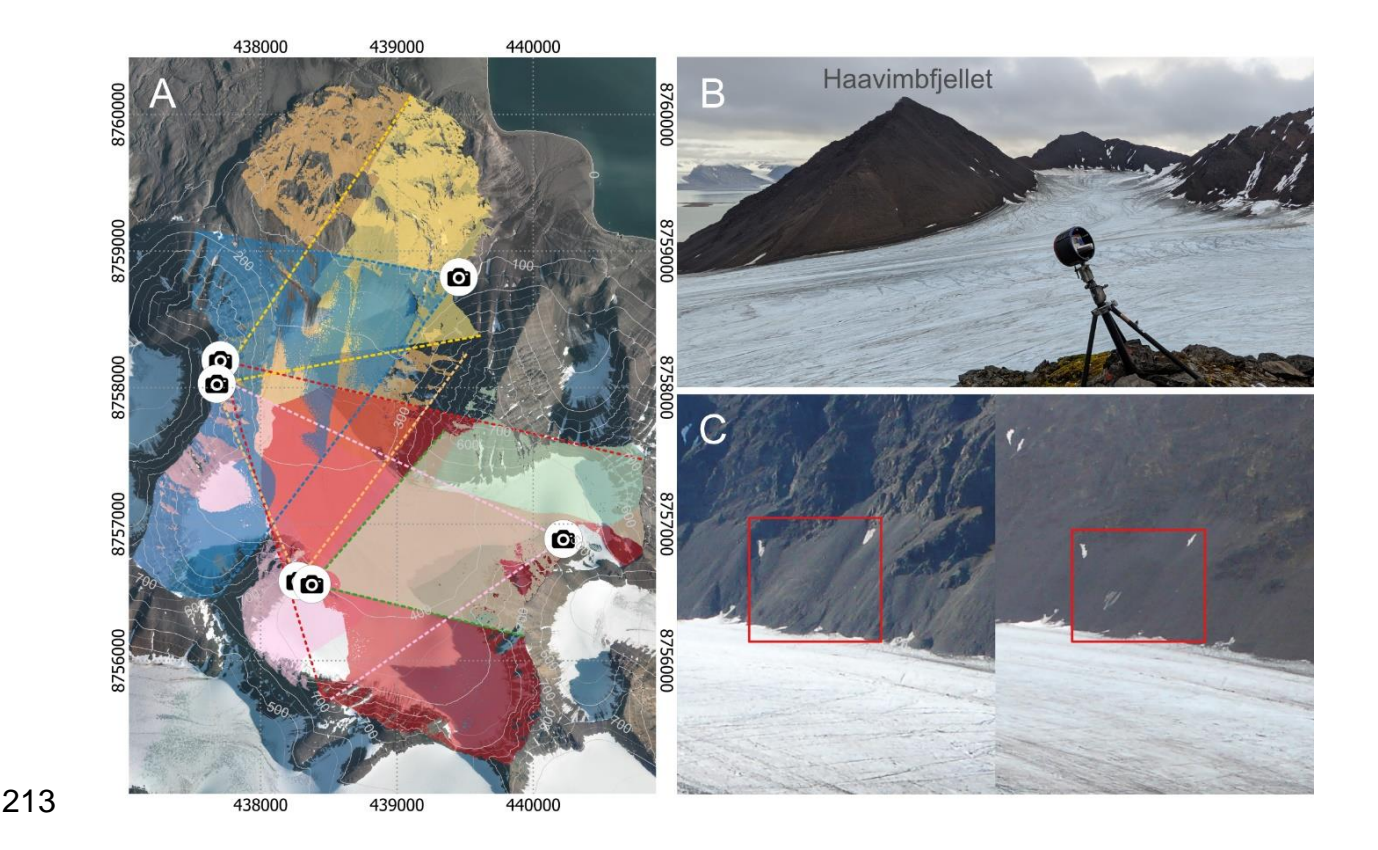


Figure 2: Automated camera system monitoring within the Austre Lovénbreen basin. A) Locations of the autonomous cameras with their individual viewshed. B Camera setup is located on a ridge southwest of the glacier basin. C) Examples of pictures taken by the northernmost automated camera system before (left; 14.08.2015) and after (right, 16.08.2015) a small debris slide located on Slåttofjellet.

The cameras provided up to three images per day depending on the polar sun cycle and meteorological boundary conditions. Typical for systems installed in such harsh conditions, data gaps are associated with temporary system or data storage failure(Bernard et al., 2013). Analysis of the more than 53.500 images was done manually, as the image's resolution for the different slopes, combined with lighting and contrast variations, did not allow for an automated analysis. Due to insufficient image resolution, the identification of landslide processes on slopes with large distances to the cameras (>1000 m) was limited to mass movement >100 m<sup>3</sup>.

#### 3.4 Meteorological data

In this study, meteorological data from two stations were used: I) the airport meteorological station in Ny-Ålesund 8 m a.s.l., roughly 5 km east of the Austre Lovénbreen basin (Maturilli et al., 2019); and II) an IPEV Automatic Weather Station located on a ridge southwest of the glacier basin, approx. 450 m a.s.l. (Bernard et al., 2013).

All meteorological variables used in this study were based on hourly measurements of temperature and precipitation. MAAT and freezing degree days (FDD) were calculated for the hydrological year, defined from 1 October to 30 September, to encompass the entire snow season. The cumulated thawing degree days (TDD) were calculated for full calendar years or till the failure date of a specific landslide (TDD @ failure), as the main energy source is solar radiation during summer (Christiansen et al., 2013). In addition to the observation sites, FDD and TDD were also calculated for different altitudes based on the daily average temperature gradient between Ny-Ålesund and the On-Site station.

Cumulative precipitation parameters were calculated for the hydrological year and the hydrological summer (1 May to 30 September) to further investigate the influence of rainfall events in the summer without considering the large quantities of snow falling during the winter months. In order to assess the influence of heavy precipitation events, the cumulative squared daily precipitation (Cum. Percipitation²) was used. Daily precipitation data is squared and consequentially summed up for the entire hydrological summer (Cum. Percipitation²hs) or till the failure date of a landslide (Cum. Percipitation²hs @ failure), assuring that higher rainfall intensities have a higher impact on the statistical analysis than represented by the cumulative daily precipitation as shallow planar debris slides are frequently triggered by extreme rainfall (e.g. Hungr et al., 2014; Peruccacci et al., 2017).

# 4. Results

249

250

251

252

253

254

255

256

257

258

259

260

261

262

263

264

265

266

267

268

269

270

#### 4.1. Landslide formation and characterisation

The Haavimbfjellet and Slåttofjellet primarily comprise low-strength and penetrative foliated phyllites of the Nielsenfjellet Formation, which act as the main starting area for rock falls (Figure 1 A). No indications of deep-seated landslide phenomena (e.g. tension cracks, graben, uphill facing scarps) within the Austre Lovénbreen basin could be identified, as commonly found in similar lithology (Agliardi et al., 2001; Macfarlane, 2009; Zangerl et al., 2010). Glacial till deposits dominate the current pro-glacial area, reworked by glacio-fluvial erosion. Sediment-mantled slopes can be observed beneath the steep rock slope sections, reaching either pro-glacial till deposits or the current glacier surface. The sediment-mantled slopes are constantly reworked by debris flows, translational debris slides, and snow avalanches in the winter. Furthermore, the high rockfall activity observed during the summer provides additional sediment influx. The slope angle of the sedimentmantled slopes varies between 34 - 40°, whereas areas of intense avalanche activity or debris flow activity, on average lead to gentler slope angles than sections predominantly formed by rockfalls. Between the in-situ bedrock and the scree, a distinct subsurface ice layer is observed in the Austre Lovénbreen basin, temporarily exposed after a slope failure. Thus, the extent of the ice layer could be mapped in areas of debris slide activity, and additional data about the scree thickness could be derived from DODs. GPR measurements by (Bernard et al., 2014) have shown that the thickness of the ice layer can reach up to several meters and is connected to

the main ice body, given contact of the glacier to the foot of the slope.

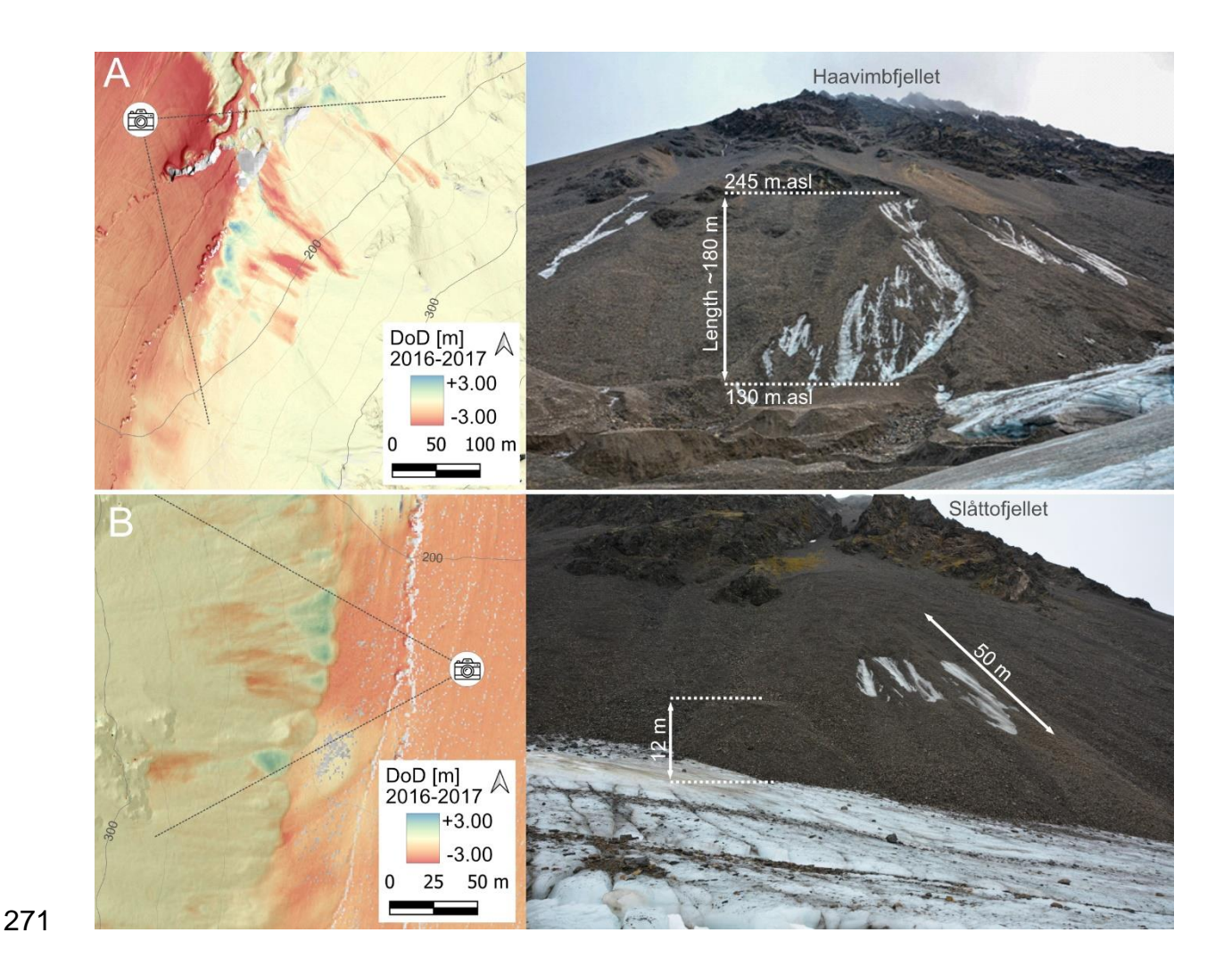


Figure 3: DEMs of Difference (TLS data: 2016/2017) and corresponding photographs of debris slides in 2017. Scarps of the debris slides are visible in the DODs, with red colours uphill corresponding to debris ablation and blue colours downhill corresponding to debris accumulation. A) Several debris slides at the snout of the glacier looking upward towards Haavimbfjellet in 2017, triggered by heavy rainfall. The sub-surface ice layer is exposed up to 115 m above the glacier surface. B) Debris slide at the slopes of Slåttofjellet triggered without any rainfall. An older debris slide deposit with approx. 12 m height can be seen south of the new deposits (which occurred prior to 2007). The debris slide south of the older deposit occurred in late 2016 (after the TLS campaign; observed through camera footage) and thus is visible in the DOD 2016-2017 but not in the provided photo.

An ice layer could also be found on sections of the talus slopes with no direct connection to the glacier since the 1970s and extends to a height up to 140 m above the present glacier elevation. Using DODs, a spatial quantification of the talus thickness above the ice layer was

possible. Hence, it was found that the overall talus thickness gradually decreases from the glacier front towards the accumulation zones until a relatively thin veneer of diamicton remains between the rock walls and the glacier ice.

Translational debris slides, and to a lesser extent debris flows, dominated the recent surface evolution of the slopes found within the Austre Lovénbreen glacier catchment during the observation period (Figure 3). However, the dominance of observed landslide processes on the slopes and sediment flux changes significantly from North to South, which also follows the overall NS-axis of the glacier. The sediment-mantled slopes can be divided into three sections: I, II, and III.

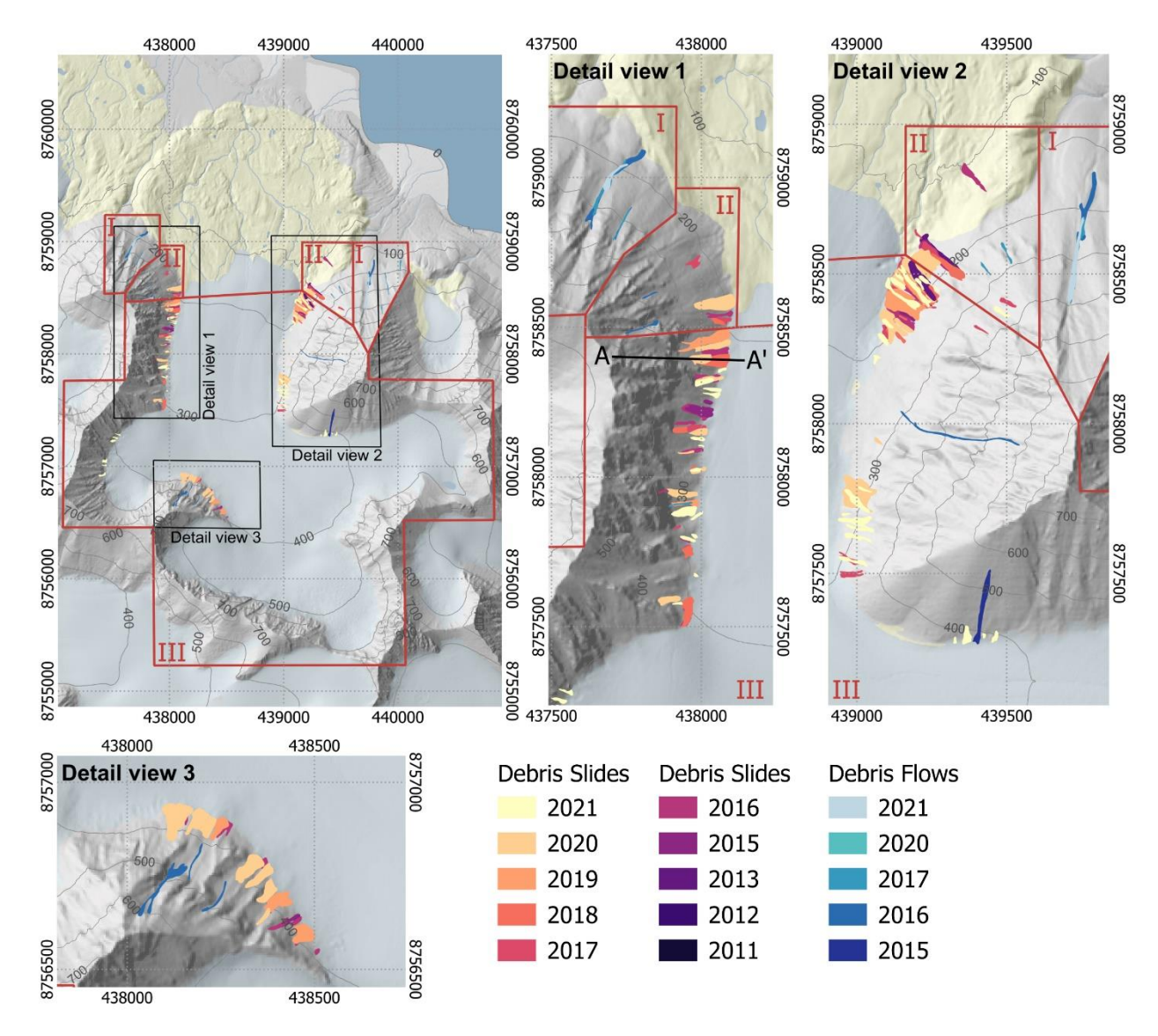


Figure 4: Overview of all observed landslides from 2011 to 2021 within the Austre Lovénbreen basin with Detail Views of the most landslide-prone slopes. The slopes were differentiated depending on the dominant landslide processes observed (Sections I, II, and III, indicated in red). Profile A-A' is indicated within Detail View 1.

**Section I)** is located beyond the extent of the lateral moraines of the Austre Lovénbreen and Midtre Lovénbreen (Figure 4). The foot of the slope has been glaciated during the maximum extent of the LIA in 1920, as seen in aerial photographs. The predominant agents of sediment transport during the observation period were debris flows (n = 11), also indicated by the much gentler slope angles (33 - 37°) found in Section I than anywhere else observed within the study area. Furthermore, the talus slopes are deeply incised by debris flow channels, which are

often framed by levees. No debris slides (n = 0) have been observed within this area, and no indication of debris slide deposits could be found.

**Section II**) has experienced gradual deglaciation since the 1970s, as seen in Marlin et al., (2017). The most dominant landslide processes are translational debris slides (n = 18) and, to a lesser extent, debris flows (n = 4). The debris flows occurred during the observation period only in the upper section of the talus slopes without reaching the valley floor (Figure 4). However, older debris cones with distinct debris flow channels and levees are located within this section. Lobate debris slide deposits are common at the foot of the slope and have been observed forming on the previous glacier surface or adjacent to the glacier.

**Section III)** comprises talus slopes in contact with the currently retreating glacier and is the largest area. The talus evolution is dominated by translation debris slides (n = 129) that can be found on all talus slopes adjacent to the current glacier extent. Runout lengths of up to 25 m (Figure 3B & 5C) could be observed forming lobate debris slide deposits. Limited debris flow activity (n = 6) was observed during the observation period, responsible for less than 2% (Figure 7 & Table 1) of the total sediment flux observed on the slopes. Debris flow channels are merely superficial ( $\leq 0.5$  m depth), and the formation of levees could not be observed.

#### 4.2. Landslide kinematics

The translational debris slides observed within the study site are defined by their shared rupture surface formed at the contact zone between the talus scree and the subsurface ice layer present within the slopes of the Austre Lovénbreen basin. As observed through the image analysis, they show a rapid first-time failure primarily initiated by heavy rainfall events.

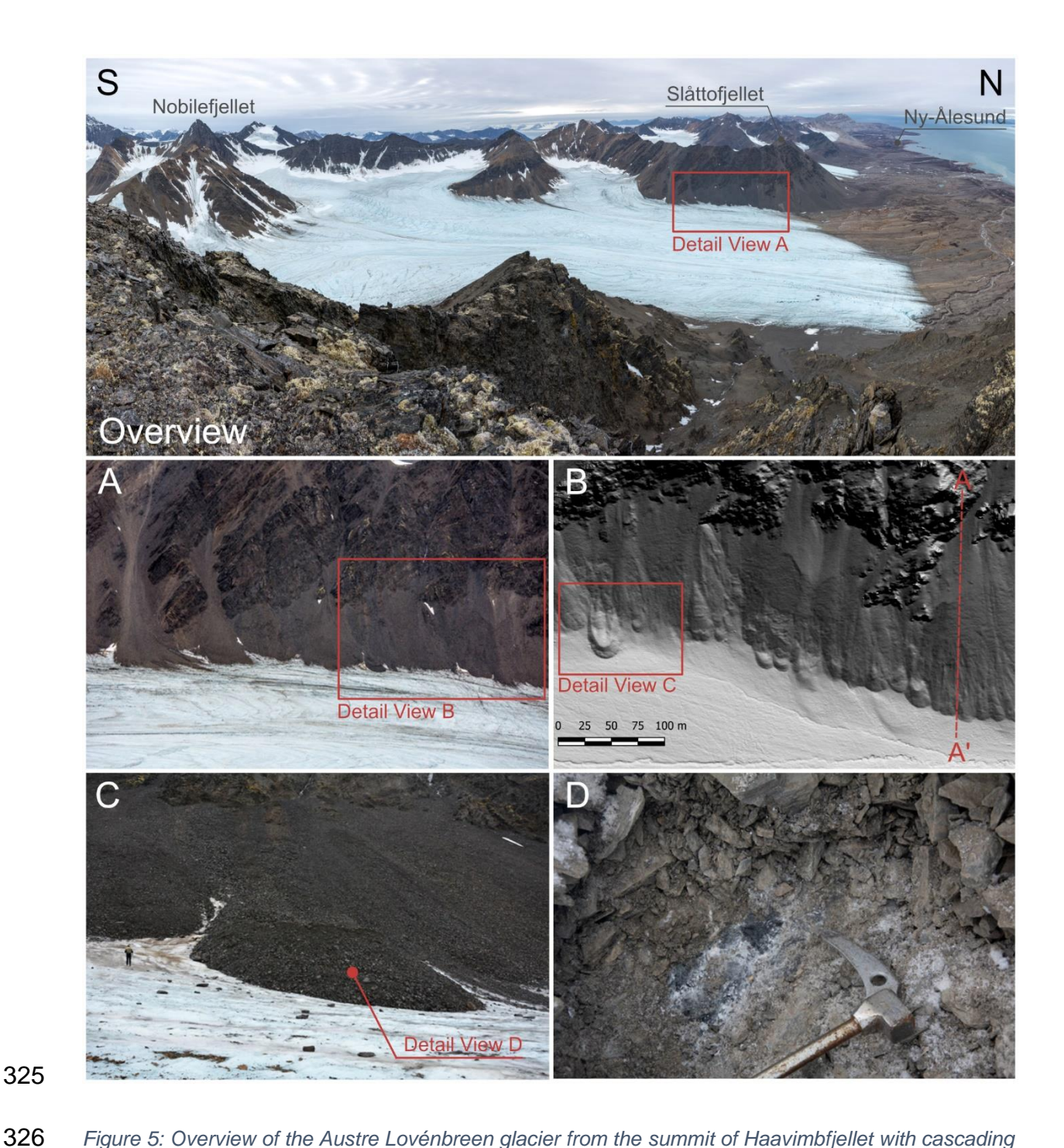


Figure 5: Overview of the Austre Lovénbreen glacier from the summit of Haavimbfjellet with cascading detail views; peaks and Ny-Ålesund are indicated. A) Photograph of the talus slopes of Slåttofjellet adjacent to the glacier. B) Hillshade of the 2017 TLS, Profile A-A' is indicated; C) Photo of the largest debris slide deposit found within the study site; person for scale. The camera system documented the initial failure in 2010. D) Trench at the front of the debris slide deposit. A solid ice core could be found after approximately 40 cm.

Due to the similarity regarding the kinematics of the observed translational debris slides, it was possible to identify five phases of debris slide induced evolution. The slope along Profile A-A' (Figure 5B) has been chosen to visualise the ongoing slope adjustment through a documented representative example as high-resolution TLS data since 2014 is available, and no previous slope failure could be identified. Thus, the entire process chain could be observed in one example. Therefore, the schematic cross-sections (Figure 6) are based on the TLS data of the observed debris slide events between 2017 and 2021. However, the thickness of the sediment layer, debris slide deposits, subsurface ice layers and the ablation of the glacier are exaggerated within the model by a factor of 1:2 to allow for better visibility. The initial prefailure topography (TLS 2016) and the 1936 topography (Girod et al., 2018) have not been altered to preserve the original slope angle and provide a conformal representation of the morphology of the pre-failure slope.

Phase 1 depicts the typical sediment-mantles (pre-failure) slope system within Section III of the Austre Lovénbreen basin. The upper section is characterised by steep rock walls consisting of low-strength phyllites with quartzite interlayers (S166/34) with scree deposits below extending onto the glacier until a thin veneer of rockfall and snow avalanche deposits remains. The glacier has lost roughly 55 m in elevation between 1936 (Girod et al., 2018) and 2016. Furthermore, (Bernard et al., 2014) have shown that a significant amount of glacier ice continues below the current extent of the talus. Field observations after several slope failures indicate the presence of a sub-surface ice layer (Figure 3) at least to an elevation of 299 m a.s.l., which is approximately 94 m above the glacier level in 2016 at this position. The full extent and thickness of the ice layer in the upper sections of the slope at Profile A-A' is not known and thus only inferred (Figure 6A).

**Phase 2** is characterised by a rapid first-time failure followed by retrogressive sliding above the main scarp. On 27.08.2017, a translational debris slide occurred at profile A-A' as the subsurface ice layer was exposed, which acted as the rupture surface. Retrogressive sliding

above the main scarp started soon after, until the exposed ice layer was covered with sediment within approximately five weeks (until 06.10.2017). The primary debris slide deposit had a volume of  $3181 \pm 318$  m<sup>3</sup> with a runout length of roughly 8 m onto the glacier surface, which formed a lobate tongue-shaped deposit. The maximum scarp height was approximately 4.20 m, as shown via DOD.

The slope failure occurred after a two-week period of increased air temperatures, with daily maxima reaching up to 11.3°C in Ny-Ålesund three days prior. Limited rainfall was observed within the two weeks prior to the slope failure. Quantifying the glacier ablation until the initial slope failure was impossible. However, the ablation at the foot of the slope between the corresponding TLS campaigns (17.08.2016 – 20.09.2017) was approximately 1.9 m.

Phase 3 corresponds to the slope readjustment after a debris slide during winter and spring (06.10.2017 until 08.07.2018 for the schematic cross-section) through the continuous retrogressive failure of the main scarp and snow avalanches in the winter, the morphological features of the main scarp are overprinted. Furthermore, an increased creep of areas above the debris slide scarp could be observed within the TLS data utilising an IMCORR approach (Fahnestock et al., 1992; Scambos et al., 1992), which may lead to a thinning of the remaining talus.

**Phase 4** comprises two main processes: I) the secondary debris slide, occurring above the initial debris slide, and II) the re-adjustment of the debris slide deposit on the glacier. Secondary debris slides can be commonly found with the Austre Lovénbreen basin triggering above the initial debris slide. The interval between two consecutive events can take several years, depending on the meteorological boundary conditions. However, a secondary debris slide occurred the following year (08.07.2018) at Profile A-A'. Following the same pattern as the initial slope failure, the sub-surface ice layer is exposed, followed by a retrogressive failure of the main scarp until the ice layer is again covered in debris. Lateral and frontal toe collapse

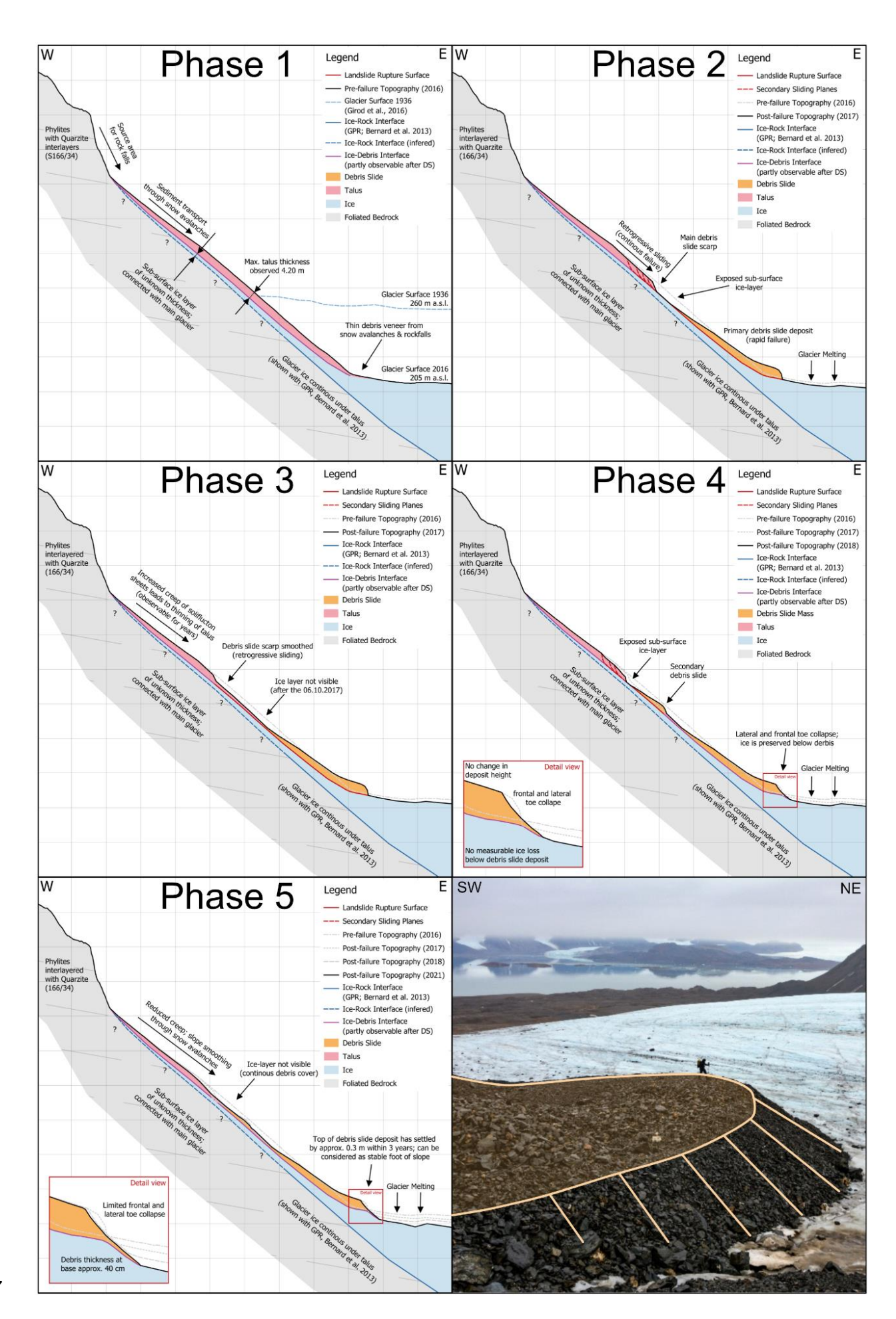
of the initial debris slide deposit was observed, forming a steep crest and a small talus apron in front of the main debris slide deposit, forming a similar morphology as a small talus-derived rock glacier (Figure 6, Phase 3). No height change was measured by TLS at the top of the deposit, indicating that the debris slide material has neither settled nor that the glacier ice below has melted.

Phase 5 corresponds to the long-term adjustment of the sediment-mantled slope towards a stable equilibrium. Continued loss of glacier ice has led to additional frontal and lateral toe collapse of the debris slide deposit at the base of the slope. Underneath this deposit, the buried glacier ice is preserved according to the thickness of the scree material above, forming a steep sediment apron (Figure 6, Phase 5, Detail view). The melting of glacier ice is interrupted under the debris deposits, which act as the temporary stable slope foot. The sediment-mantled slope further adjusts to the new slope angle defined by the debris slide deposit. Snow avalanches further erode debris slide features (e.g. scarps) on the slope. The increased creep above the slope failures reduces to pre-failure velocities.

At Profile A-A' from the debris slide deposit, a scree apron with a height of approximately 5 meters and a thickness of 40 cm had formed after four years. The top of the debris slide deposit has settled at the crest by a maximal 0.3 m within three years and can be considered stable. The largest debris slides (e.g. longest runout lengths) located on the glacier may show flow features after several years, as the glacier ice drags the deposit along the main flow direction. Thus, larger deposits may bear strong morphological similarity to small protalus rock glaciers, except for a core of glacier ice. Debris slide deposits show no measurable creep if located beyond the extent of the Austre Lovénbreen glacier.

Figure 6: Schematic cross-sections depicting the slope evolution at Profile A-A' between 2016 and 2021 with an example picture of the largest debris slide deposit within the Austre Lovénbreen basin. Phase 1) State of the pre-failure slope found in 2016. The extent of the sub-surface ice layer is partially known from studies by Bernard et al. (2013), and the state of the glacier in 1936 (Girod et al., 2016) is indicated.

Phase 2) Initial translational debris slide observed on 27.08.2017, exposing the sub-surface ice layer. Retrogressive sliding was observable for several weeks after. Phase 3) Slope readjustment between 06.10.2017 and 08.07.2018 through the continuous retrogressive failure of the main scarp and snow avalanches. Phase 4) Secondary translational debris slide on the upper section of the slope. Lateral and frontal toe collapse of the initial debris slide deposit protects the glacier ice from melting. Phase 5) Long-term adjustment of the sediment-mantled slope towards a stable equilibrium between 2018-2021. Continued loss of glacier ice has led to additional frontal and lateral toe collapse of the debris slide deposit at the base of the slope. Underneath this deposit, the buried glacier ice is preserved.



#### 4.3. Magnitude and frequency of landslide events

During the observation period, 171 distinct landslide events could be identified. These encompass 147 translational debris slides, 21 debris flows and 3 rock falls (>1m³). Smaller rockfall events were commonly observed during the field campaigns, but individual events could not be differentiated via the TLS data. Debris slides were responsible for approx. 96% (V<sub>Debris Slides</sub>: 122889.3 m³) of the entire sediment flux observed at the slopes of the Austre Lovénbreen basin (Table 1). Thus, debris flows act as a minor agent of sediment transport (V<sub>Debris Flows</sub>: 4981.7 m³), except within Section I (Figure 4).

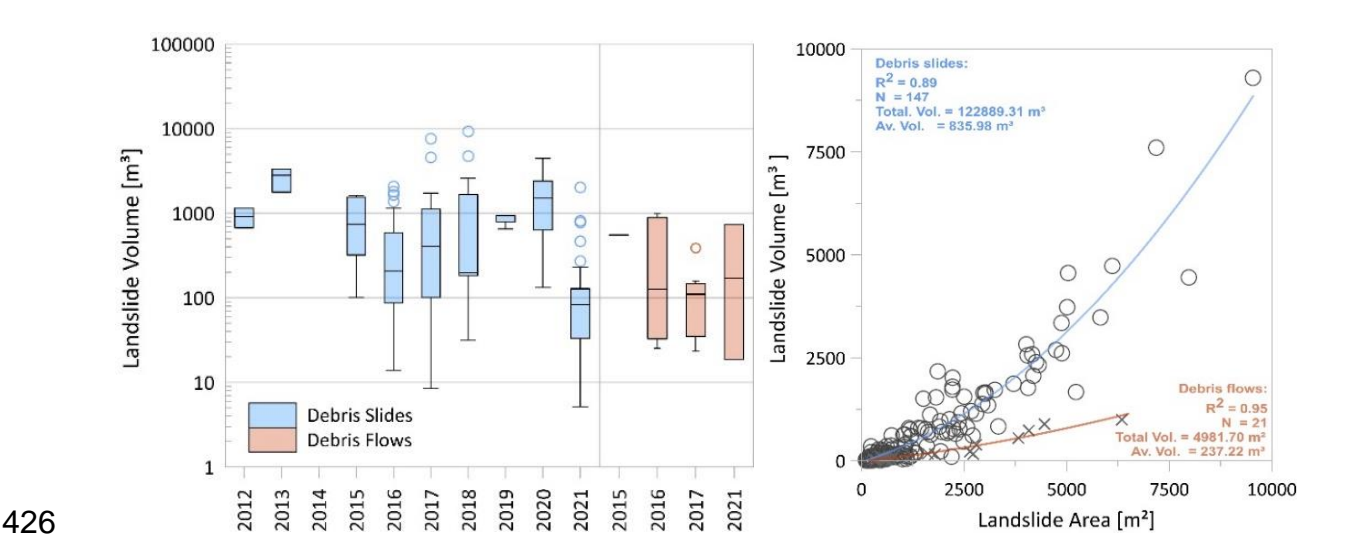


Figure 7: Boxplot of all observed landslides per year (left) and the relationship between the landslide volume and area (right).

The observed landslides vary strongly in volume, extent, and depth throughout the years, with debris slides ranging from  $12.5 \pm 4.9 \text{ m}^3$  to  $9295.8 \pm 502.5 \text{ m}^3$  with an average volume of  $835.9 \text{ m}^3$  and debris flows from  $18.8 \pm 5.4$  to  $996.4 \pm 106.5 \text{m}^3$  with an average volume of  $237.2 \text{ m}^3$  (Figure 7). However, there is a strong correlation between the area and volume of landslide processes due to the subsurface ice layer acting as the common rupture surface plane (Figure 7, right).

The frequency and magnitude of individual landslide events greatly fluctuate within the observation period (Figure 7, left). However, a significant increase in the overall landslide activity ( $R^2 = 0.57$ ; P-Value = 0.0068) can be observed between 2011 and 2021 (Figure 8).

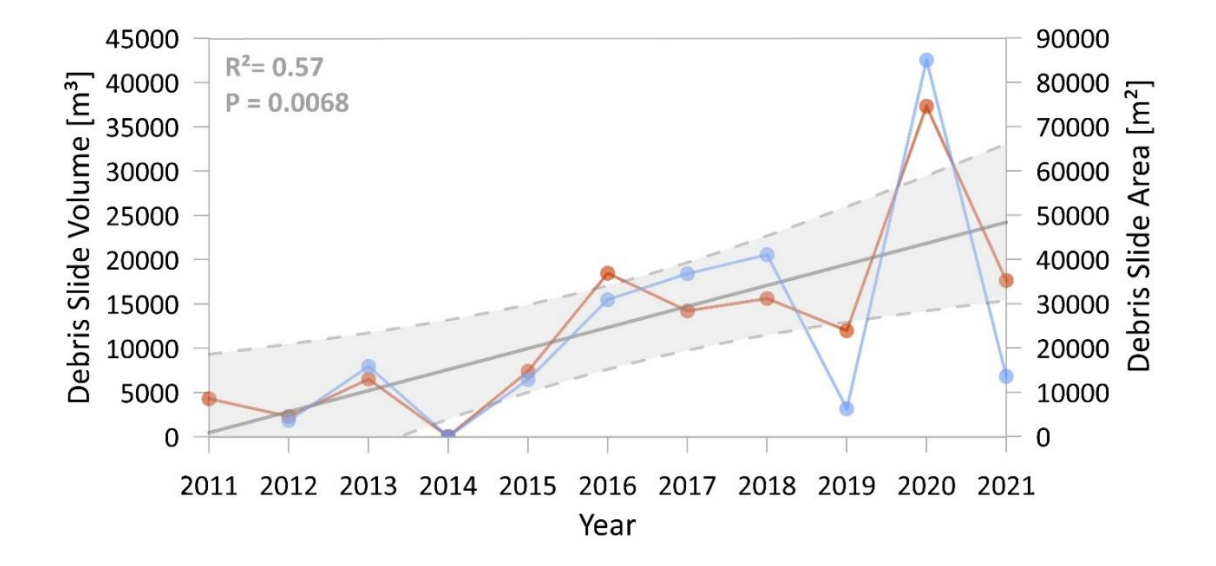


Figure 8: Total Debris slide area (red) and volume (blue) per year observed within the Austre Lovénbreen basin. Linear fit with a 95% confidence interval for the debris slide area is indicated in grey.

Table 1: Landslide volume, area and quantity for debris slides and debris flows observed between 2011 and the TDD, cumulative daily precipitation for the hydrological summer (Cum.  $P_{hs}$ ) and cumulative daily squared precipitation for the hydrological summer (Cum.  $P_{hs}^2$ ). Debris slide volumes have been calculated using a spatially variable LOD (confidence interval of 95%).

Year	Debris Slide Area [m²]	Debris Slide Volume [m³]	n	Debris Flow Area [m²]	Debris Flow Volume [m³]	n	TDD [°C]	Cum.P <sub>hs</sub> [mm]	Cum.P <sup>2</sup> hs [mm]
2011	8525.9	No Data	4	0	0	0	630	148	1023
2012	4521.8	1827.6 ± 227.8	2	0	0	0	545	135	1120
2013	12946.2	7943.3 ± 637.8	3	0	0	0	553	264	2381
2014	0	0	0	0	0	0	449	242	2769
2015	14716.2	6445.8 ± 802.2	8	3823.9	551.6 ± 109.7	1	616	166	1507
2016	36852.5	15473.9 ± 1718.8	36	18604.8	2445.4 ± 327.6	8	687	243	3667
2017	28373.1	18407.1 ± 1202.4	15	8970.1	1064.1 ±193.9	9	649	220	3943
2018	31150.9	20557.5 ± 1440.1	13	0	0	0	624	269	3912
2019	23910.1	3172.0 ± 367.1	4	0	0	0	595	126	779
2020	74570.7	42524.6 ± 5563.4	27	0	0	0	729	143	856
2021	35234.6	6829.1 ± 1308.2	39	6050.2	920.4 ± 254.8	3	547	152	1991

# 4.4. Impact of meteorological parameters on landslide formation

Throughout the monitoring programme, the date of failure of 106 translational debris slides could be identified within a range of hours or days, depending on meteorological conditions (e.g., clouds, fog, excessive rain), through the long-term monitoring network.

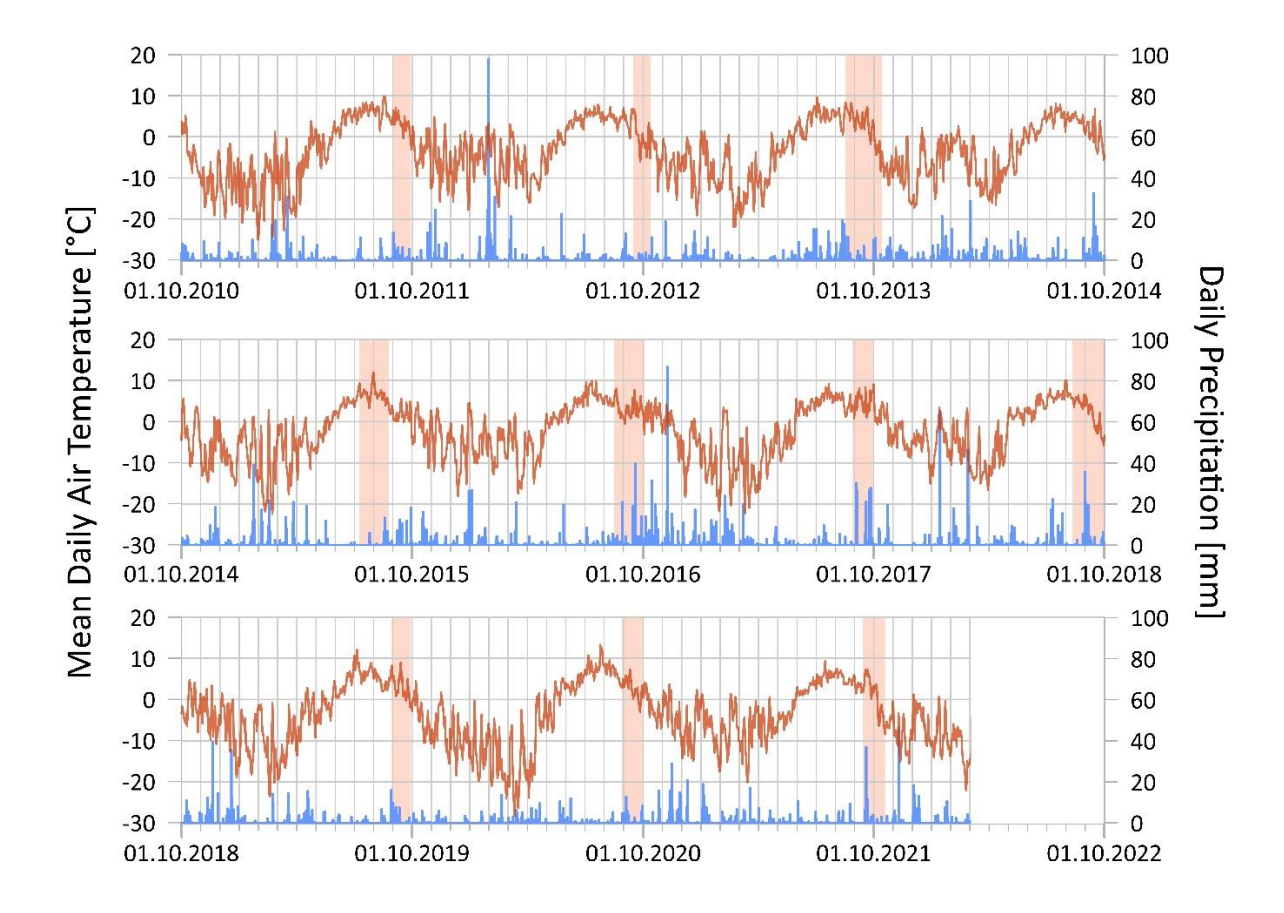


Figure 9: Daily mean air temperature and daily precipitation at the Ny-Ålesund meteorological station from 2010-2021. Periods of observed landslide activity are indicated in red.

The time of failure for the observed debris slides ranges from late August till the beginning of October (Figure 9), when the maximum thaw depths are reached. However, single events could also be observed in the lower altitudes during July. No in-situ data for the thaw depth was available within the slopes. Thus, the annual maximum thawing degree days measured in Ny-Ålesund (TDD) serve as a proxy value to quantify the overall heat input during the year projected onto the entirety of the Austre Lovénbreen basin (Figure 10). The majority of

precipitation at Ny-Ålesund during the hydrological year falls during the winter period as snow. Thus, the cumulative precipitation during the hydrological summer is better suited to quantify the impact of precipitation on landslide formation within the Austre Lovénbreen basin (Figure 10).

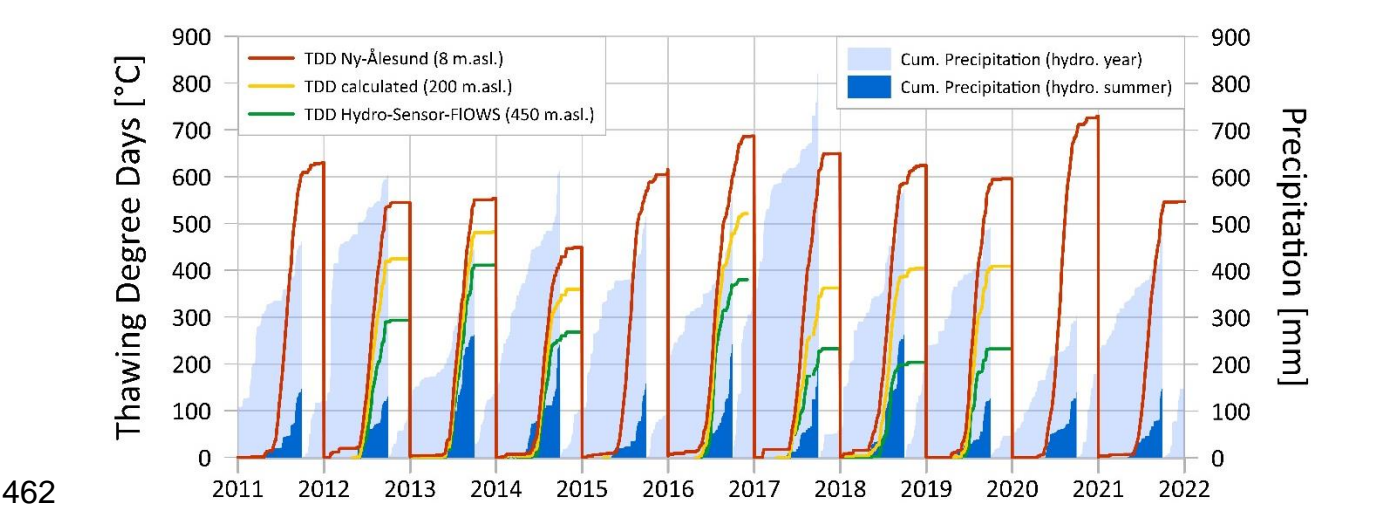
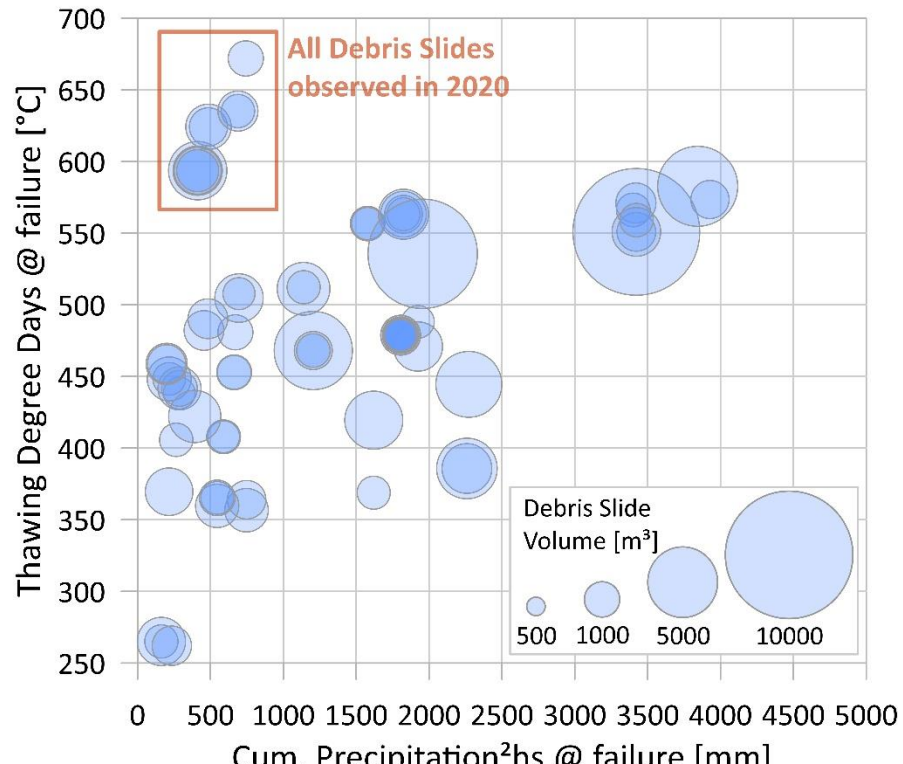


Figure 10: Thawing Degree Days measured at Ny-Ålesund (8 m a.s.l.), the IPEV Automatic Weather Station within the Austre Lovénbreen basin (approx. 450 m a.s.l.), and a TDD calculated exemplary for 200 m a.s.l. based on the height-dependent temperature gradient of the available datasets and the cumulative precipitation for the hydrological year and summer.



Cum. Precipitation<sup>2</sup>hs @ failure [mm]

469

470

471

472

473

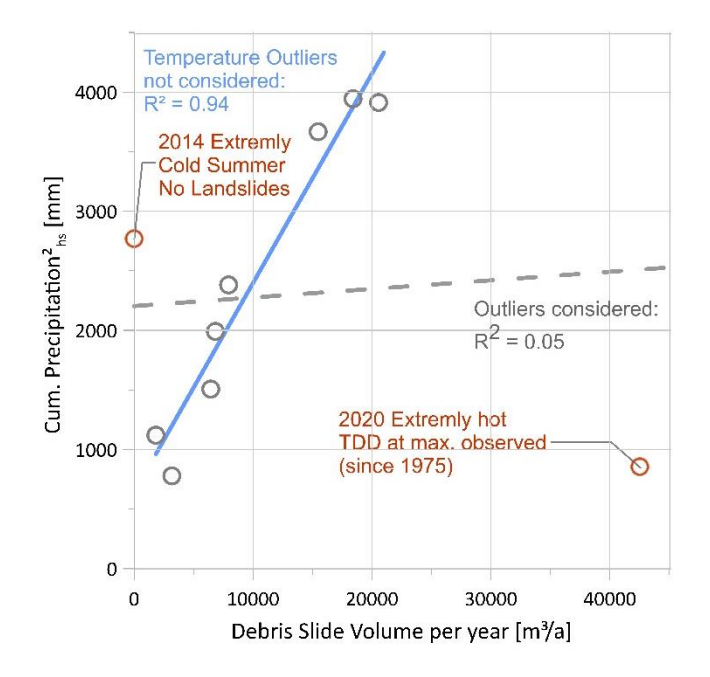
474

475

476

Figure 11: Thawing degree days (TDD @ failure) and cumulative squared daily precipitation during the hydrological summer (Cum.Precipitation<sup>2</sup><sub>hs</sub> @ failure) were calculated for the date of the initial slope failure of 106 individual debris slides observed between 2011-2021.

A general trend between debris slide volume and meteorological boundary conditions can be observed for individual debris slide events. Higher temperatures (TDD @ failure) and rainfall intensities (Cum.Precipitation2hs @ failure) observed during the years lead to larger debris slides. Furthermore, a cluster of primary temperature-induced debris slides occurring in 2020 can be observed (Figure 11).



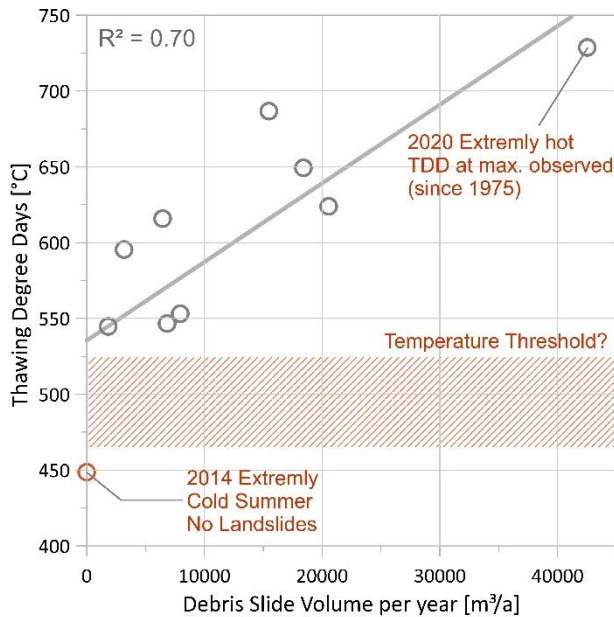


Figure 12: Impact of rainfall on debris slide formation.

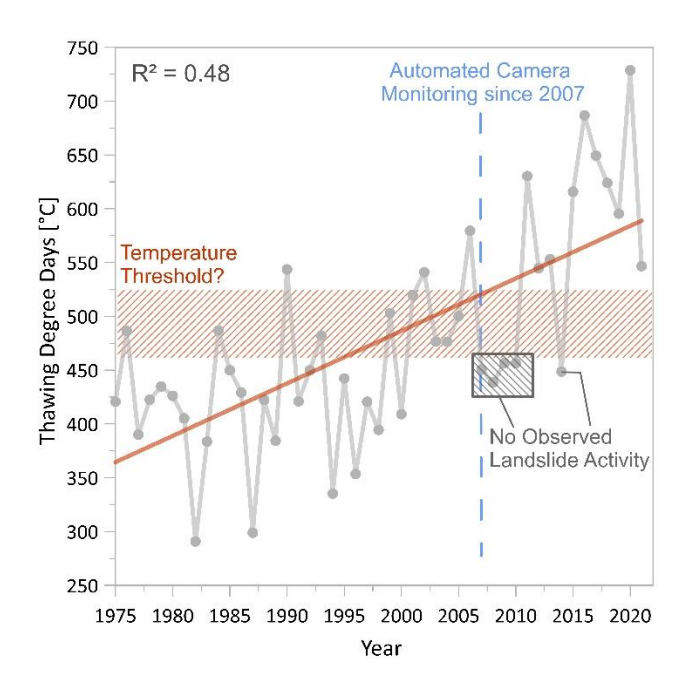
Cumulative squared daily precipitation (hydro.

Summer) and debris slide volume per year between

2011 and 2021.

Figure 13: The thermal dependency of debris slide formation with the Austre Lovénbreen basin. No debris slides were observed within a year when the TDD was below 545 °C.

When analysed per year, a strong correlation (R² = 0.94) between the cumulative squared daily precipitation (Rainfall² hydro. summer) and the total landslide volume per year could only be found when temperature outliers were not considered (Figure 12). Since 2007, a TDD of at least 545°C had to be reached for any debris slides to occur, indicating a thermal threshold necessary for debris slide formation within the Austre Lovénbreen basin beyond heavy rainfall events (Figure 13). This is outlined from 2007 till 2010 and 2014, when no debris slides were observed (Figure 14), even though a potentially sufficient amount of rainfall was given (Figure 12). Thus, a temperature threshold necessary for heavy rainfall events to trigger an initial slope failure can be assumed. Furthermore, as in 2020, debris flows occurred without observable rainfall prior to the slope failures (meteorological stations; automated camera network) beyond a TDD of 700 °C.



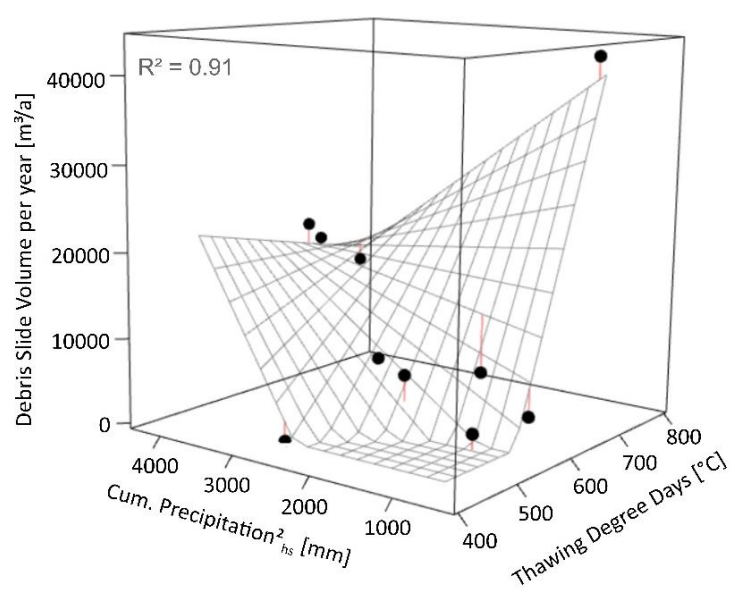


Figure 14: Increase of TDD in Ny-Ålesund since 1975. Since implementing the automated camera network, only five years were observed without debris slide activity (TDD below 545 °C), indicating a temperature threshold for debris slide activity.

Figure 15: Impact of temperature and (TDD) and precipitation (Cum. Precipitation<sup>2</sup><sub>hs</sub>) on the debris slide formation per year ( $R^2 = 0.91$ ). Residuals are indicated in red.

Ultimately, the best description of the increase in debris slide magnitude is achieved for all data points (2012-2021) with a linear model that includes both temperature (TDD) and heavy rainfall (Cum. Precipitation<sup>2</sup>hs) variables (Figure 15). The negative interaction term shows that the effect of temperature and rainfall variables is less than the sum of the individual effects.

#### 5. Discussion

#### 5.1 Data limitations

In the present study, the slopes of the Austre Lovénbreen glacier basin were monitored with terrestrial lidar for a 10-year period (2012-2021) and autonomous cameras for 15 years (2007-2021). After a stable period from 2007 to 2011, slope failures could be observed almost every year by TLS and the automated camera network. Particular advantages and deficiencies of the applied remote sensing techniques became evident in our study.

The multi-temporal TLS data allowed us to detect and quantify complex and incremental terrain changes between individual TLS campaigns within a distance-variable level of detection at a confidence interval of 95% (LOD95%). However, the limited temporal resolution of TLS (i.e. one measurement per year) does not provide sufficient information to investigate the trigger mechanisms of slope processes. Whilst the automated camera network's main purpose was to evaluate snow cover in the most remote and inaccessible areas (Bernard et al., 2013; Friedt et al., 2023), it proved particularly effective for qualitative landslide detection. Daily camera images provided key information about the failure date, duration, trigger mechanisms, and kinematics of landslides, as well as additional qualitative weather observations within the study area while increasing the observation period by five years. Data gaps within the TLS data could also be amended as the failure dates of almost all large translational debris slides (>2000 m³) could be identified. Thus, the temporal limitations of the TLS data were reduced significantly.

The visual detection of landslide processes was primarily limited by data gaps resulting from temporary system or data storage failures of individual cameras and camera resolution. Given that landslides of lesser size or limited visual impact were hard to distinguish from lighting and contrast variations between individual images. Whilst it was possible to identify the event time of 106 translational debris slides (n = 147) within the range of hours or days depending on the

visibility during or after rain events (e.g. fog, cloud cover), only 7 debris flows (n = 21) and no rock falls could be identified. This is unsurprising due to the differences in the average volume between the different landslide types, as shown by the good correlation between the landslide area and size within the study area (Figure 7). While small-scale landslide events (≤ 100 m³) at larger distances from the cameras are often difficult to detect, it must be emphasised that the network was originally not designed for this task. Furthermore, the 49 small-scale events (≤ 100 m³) between 2012 and 2021 only accounted for approx. 2% of the total paraglacial sediment transfer via landslides. This may introduce certain data biases within the investigation of trigger mechanisms and magnitude on an individual level (Figure 11) but does not affect the statistical analysis of the annual landslide activity (Figures 12, 13 & 15) as the quantification of landslide processes was derived from the TLS data. The identification of landslide processes prior to available TLS data based solely on the automated camera network as the ALS-Data from 2010 (NPI, 2014) proved insufficient to quantify landslides within the level of detection. Thus, only the landslide areas of the four translational debris slides in 2011 were mapped (Table 1).

# 5.2 Spatiotemporal variation of dominant landslide processes within the paraglacial period

Across the Austre Lovénbreen Basin, translational debris slides were the dominant agent of paraglacial sediment transport (96%) between 2012 and 2021, modifying the steep sediment-mantled slopes (Figure 7 & Table 1). With increasing distance from the glacier terminus, a spatial shift of the dominant landslide processes from debris slides (Section III) towards debris flows (Section I) could be observed (Figure 4). Mercier et al., (2009) described a lateral succession of different landslide processes at *Colletthøgda* (7.5 km north-east from the study site), with translational slides in proximity to the glacier that are succeeded by debris flows, gullying and rill erosion during later stages of paraglacial slope evolution.

Debris flows are generally considered the primary source of erosion and sediment transport acting within the paraglacial period (Ballantyne, 2002; Ballantyne & Benn, 1994; Chiarle et al., 2007; Curry, 1999; Evans & Clague, 1994; Owen, 1991). However, modification of steep sediment-mantled slopes by translational debris slides may be extensive given recent glacier retreat (Ballantyne, 2002) and thus is limited by a temporal and spatial component. Similar observations were made on ice-cored scree slopes and moraines in Svalbard (Mercier et al., 2009), the Canadian Rocky Mountains (Mattson & Gardner, 1991), and the Vestfold hills in East Antarctica (Fitzsimons, 1996).

Given the consensus that the rate of primary paraglacial sediment transfer reaches a peak soon or immediately after deglaciation and declines thereafter (Ballantyne, 2002), as expressed by the exponential exhaustion model of paraglacial sediment reworking (Ballantyne, 2002; Cruden & Hu, 1993) or similar relaxation curves (Church & Ryder, 1972), translational debris slides can be the dominant agent of the primary sediment transport on paraglacial slope systems. Due to their spatiotemporal connection to glacier downwastage and retreat, as shown within a rapidly changing environment such as the Austre Lovénbreen basin.

The paraglacial sediment transport pre-dominantly by translational debris slides within the Austre Lovénbreen basin indicates that the slope system is generally at an early stage of development. Observed debris flows, and associated landforms (e.g., levees and debris cones) only dominate slope sections (Figure 4, Section I). The impact of debris flows was marginal for the entire basin  $(3.9\%; 4981.7 \, \text{m}^3 \pm 886.2 \, \text{m}^3)$  and was primarily located in Section I  $(2.9\%; 3709.9 \pm 644.9 \, \text{m}^3)$ . Thus, Section I may present a more advanced and to a degree stable stage of slope development.

The initial strong sediment flux by translational debris slides is followed by a decline of available unstable sediment sources until only sporadic debris flow activity remains. Our

observation fits well into the concept of an exponential exhaustion model of paraglacial sediment reworking. A decline of paraglacial sediment transport with increasing distance to the glacier terminus and shifting dominant mass wasting processes was also observed through vegetation studies at the nearby Colletthøgda and was connected to the decay of dead-ice within the slopes (Mercier et al., 2009).

The impact of translational debris slides on paraglacial slope modification may also be underestimated, given a lack of data with a high spatiotemporal resolution. Translational debris slides and associated landforms (e.g. scarps, deposits) are overprinted or eroded by other processes. Erosion of debris slide landforms by snow avalanches was observed between 2018 and 2021 at Profile A-A' (Figure 6, Phase 5) and the lack of translational debris slides or older debris slide deposits within Section I may be caused by an overprint through other processes, such as debris flows and snow avalanches.

# 5.3 Landslide initiation and trigger mechanisms

Different meteorological parameters control landslide processes (Crozier, 2010; Gariano & Guzzetti, 2016; Patton et al., 2019) and thus, from the overlying climate (Gariano & Guzzetti, 2016; Matthews et al., 2018; Patton et al., 2019; Soldati et al., 2004). Factors such as topography, lithology, geological structures, in-situ stresses, groundwater flow, glacial conditioning, permafrost and availability of sediment sources define the pre-disposition for potential slope instabilities (Crosta et al., 2013; Rechberger et al., 2021). Landslide trigger mechanisms can be further correlated to climatic conditions or their fluctuation, chiefly temperature and precipitation (Ballantyne, 2002; Crozier, 2010; Dhakal & Sidle, 2004; Gariano & Guzzetti, 2016) and thus also other correlated processes (e.g. permafrost degradation, glacier retreat). Additionally, recent deglaciation may impact landslide initiation through reduced lateral support, stress-redistribution, dead-ice outcropping, or the rapid melting of ice-cored bodies (Ballantyne, 2002; Mercier et al., 2009). However, quantifying the impact of

meteorological factors on landslide processes is challenging as combined effects may have different and often contrasting effects (Gariano & Guzzetti, 2016; IPCC, 2014) depending on the slope system and landslide type.

592

593

594

595

596

597

598

599

600

601

602

603

604

605

606

607

608

609

610

611

612

613

614

615

616

However, studies in comparable paraglacial environments concluded that paraglacial sediment transfer by landslides occurs annually, and the spatial distribution of dead ice within sediment-mantled slopes is the main control of paraglacial sediment transfer (primarily debris flows) rather than meteorological events (Ballantyne, 2002; Ballantyne & Benn, 1994; Mercier et al., 2009). By contrast, we could show that meteorological factors primarily explain the frequency and magnitude of landslide processes during a 10-year observation period (Figure 15). The spatial occurrence and extent of the subsurface ice layer within the slopes is the main predisposition factor determining the dominant landslide process (Figure 4; Sections 1 and 3). Heavy rainfall events during the hydrological summer are the main triggering factor contributing to the magnitude and frequency of translational debris slides (Figure 12). In contrast, the temperature regime during a given calendar year (expressed by TDD in this study) is the primary control for debris slide initiation (Figures 13 & 14). As below a certain temperature threshold (TDD ~545 °C), no landslides could be found between 2007-2021, even though heavy rainfall events were observed within the summer. A cluster of debris slide events without any unambiguous trigger (rainfall) occurred in 2020 when the warmest summer period was registered (TDD >700 °C). Therefore, the cause may be due to increased melting of the subsurface ice layer found within the slopes, given sufficient subsurface heat transfer (Figure 11). Similarly, Mercier et al. (2009) described extensive erosion rates primarily caused by meltwater-induced translational slides and dead ice scouring in areas adjacent to the glacier

Furthermore, Mattson & Gardner (1991) identified meteorological factors (e.g. heavy rainfall; temperature increase) to be contributing factors for the formation of rapid translational debris

margin, thus also implying a weather-induced component.

slides along an ice layer within slopes adjacent to the Boundary Glacier (Alberta, Canada). They associated periods of warm weather, most conductive to ablation of the glacier with 5 observed translational debris slides (n = 25). However, they noted that these temperature-triggered debris slides were generally of lesser magnitude as they only contributed 14% to the total sediment flux from the slopes. At the Austre Lovénbreen only 9 translational debris slides (n = 107) were identified as temperature-induced with above-average magnitudes (1131.6  $\pm$  150.1 m³) (Figure 11, indicated in red).

Given that the rupture surface of all translational debris slides was the clearly observable icedebris interface (Figure 6) and a certain temperature threshold needed to be reached before debris slides can form (Figure 14). Based on our observations, it can be assumed that the annual thaw depth has to penetrate the ice layer in order to trigger debris slides. Furthermore, the observed translational sliding characteristics indicate that the planar ice-debris interface is the main weakness zone most likely affected by annual thawing and water infiltration. The water source may be either from heavy rainfall events or meltwater from the ice layer, given sufficient subsurface heat transfer within a year.

By contrast, debris flows were only detected during 4 years of the 10-year period of available TLS data (Figure 7). Observation via the automated camera networks showed that they occurred erratically after rainfall events of varying intensity. However, years with above-average rainfall during the summer period showed increased debris flow activity (Table 1). Statistical correlation with rainfall activity or individual heavy rainfall events was limited due to the short observation period (only four years with debris flows). Nonetheless, debris flow initiation and magnitude are closely linked to heavy rainfall events in mountainous regions and the usage of rainfall thresholds as minimum conditions for debris-flow triggering is widely accepted (Hübl, 2018; Hürlimann et al., 2019; Peruccacci et al., 2017; Stiny J, 1910; Zimmermann & Haeberli, 1992).

Case studies in comparable paraglacial environments, such as the Fåbergstølsdalen (Ballantyne & Benn, 1994) and Colletthøgda (Mercier et al., 2009) found that paraglacial sediment transfer by debris flows occurs annually on steep sediment-mantled slopes and is not dependent on meteorological extreme events. However, the comparability of those case studies may be limited as the annual average rainfall found at the Fåbergstølsdalen (Central Norway) is considerably higher than at Kongsfjorden. Thus, it is more likely that rainfall thresholds could have been reached every year at the Fåbergstølsdalen. Whereas the observation period at Colletthøgda was limited and fieldwork was only conducted in 1996 and 2004.

Debris flows initiated by translational debris slides (debris flowslide after the Varnes classification; Hungr et al. (2014)), as seen by Ballantyne & Benn (1994) at the Fåbergstølsbreen (Norway), could not be observed within the study area. As debris flowslides are caused by excess pore-pressure or liquefaction of material originating from the landslide source (Hungr et al., 2014), the lack of rainfall in the Kongsfjorden area may impede their development.

Infiltration and in-situ melting at the debris-ice interface may reduce the shear strength and the grain interlocking-dependent cohesion of the debris. The water that fills the pore space of the sediment body after rainfalls may also increase shear stress. However, rainfall accumulation at the interface depends on the sediment cover's permeability and depth (Mattson & Gardner, 1991). Snow melt and heavy rainfall events during the early summer did not affect translational debris slide initiation, as percolation of rainwater within a frozen debris body may be limited. However, non-conductive heat transfer by rainwater during the spring and summer may be a contributing factor. Furthermore, the continuous downwastage of the glacier at the foot of the slopes did not cause any translational debris slides but rather led to an adjustment of the slope foot by creep processes, as observed from 2007 to 2011 and in 2014.

# 5.4 Spatial extent and origin of sub-surface ice layer within the sediment-mantled slopes

Due to the difficulty of the terrain, the spatial extent of the subsurface ice layer within the sediment-mantled slopes could only be investigated at fresh scarps of the debris slides, where the ice is outcropping. Thus, it is currently unknown if the ice within slopes unaffected by translational debris slides (e.g., Section 1, Figure 4) has either decayed or accumulated a sufficient protective debris cover.

Reconstructions of the Austre Lovénbreen glacier based on aerial imagery from 1923 (Mittelholzer, 1923) and 1936 (Girod et al., 2018) show the glacier elevation up to 75 m (55 m at Profile A-A'; Figure 6A) above the current level. The Little Ice Age (LIA) ended on Svalbard in the 1920s (Svendsen & Mangerud, 1997) and studies have shown that the LIA corresponds well with the maximum glacier extension of the Holocene (Błaszczyk et al., 2009; Farnsworth et al., 2020; Humlum et al., 2005; Martín-Moreno & Allende-Álvarez, 2016; Snyder et al., 2000). Thus, the reconstructed heights from 1936 potentially show the state of the Austre Lovénbreen close to the maximum extent within the Holocene. Therefore, a glacial origin of the subsurface ice layer up to 70 m above the current glacier level can be assumed, as also shown by investigations by Bernard et al. (2014) based on Ground Penetrating Radar.

Indicating that the dead ice within the lower sections (max. glacier elevation) of the slopes is at least 85 years old and potentially much older in the upper section. Whereas the conceptual model of morphological slope evolution based on vegetation studies at Colletthøgda assumed that the melting of the last dead-ice bodies (10-150 m a.s.l.) occurs roughly 35 years after deglaciation (Mercier et al., 2009).

Formation of segregation ice within the debris could be responsible for the ice within the upper slopes of the Austre Lovénbreen basin. However, a glacial origin cannot be entirely discarded, considering the thickness and continuity of the observed ice layer up to 245 m a.s.l. within the

sediment-mantled slopes at the current glacier terminus (~130 m a.s.l.) (Figure 3). Thus, ice sampling and age dating are required to assess the origin of the ice layer and the spatial extent within Section 1 (Figure 4).

## 5.5 Temperature thresholds on landslide activity

The duration and intensity of the thawing period and thus the maximum thaw depth at the end of the summer thaw season (ATD) was identified as the primary control for initiating debris slides (temperature threshold; TDD ~545 °C). Whereas the average ATD or the maximum depth of the 0 °C isotherm for two consecutive years is used to define the active layer thickness (ALT) (Schaefer et al., 2011), only the annual maxima (ATD) is relevant as a trigger factor for translational debris slides. Several studies have shown the dependence of ALT, and thus ATD, on meteorological factors (i.e. precipitation, snow cover, mean annual air temperature and variation) and specific site parameters (i.e. substrate, topography, hydrology, vegetation) (Strand et al., 2021; Zhang & Stamnes, 1998). The depth of thaw is usually assumed to be controlled by conditions during the thawing season and thus is often positively correlated with TDD, as shown by the simplified variant of the Stefan equation:

708 Equation 1 
$$Z = E\sqrt{TDD}$$

where Z is the depth of thaw; TDD the Thawing Degree Days (TDD); and E is the edaphic factor, which is a scaling parameter summarising site variability and can be calculated given a known Z and TDD for a specific location (Hinkel & Nicholas, 1995; Stefan, 1890; Strand et al., 2021). Site-specific E-values for the Austre Lovénbreen basin were calculated using either the maximum TDD within a year (TDD) or the Thawing degree days during the initial triggering of a translational debris slide (TDD @ failure). The thaw depth was assumed to be equivalent to the maximum thickness of the dated 106 landslides, given that the rupture surface was alone the planar subsurface ice layer. However, the calculated E values varied strongly, and no correlation was found with landslide thickness. Considering the relative homogenous

material found on the sediment-mantles slopes, the main reason might be due to snow cover variations, the impact of rainfall on the non-conductive heat transfer processes by water during a year and the different landslide trigger mechanisms (e.g. rainfall or meltwater-induced). Assessment of the spatial variation of these factors would require a 3D modelling approach in combination with an expansion of the current monitoring network. Nonetheless, a strong correlation between the TDD and landslide activity during a year (R = 0.70) could also be observed within the Austre Lovénbreen basin.

Furthermore, a potential temperature threshold can be assumed based on the observations between 2007 and 2021. Whilst a definition of a sharp temperature threshold for potential landslide activity within the Austre Lovénbreen basin is not possible due to the limited dataset, a transition zone between years of landslide activity (minimum TDD~545°C) and inactivity (TDD~450°C) could be found (Figures 13 & 14). Debris flows were also not observed in years below a TDD of ~545°C. However, this may be due to the above-explored data biases affecting smaller landslide phenomena between 2007 and 2011.

The impact of winter air temperatures, expressed by the Freezing Degree Days (FDD), on landslide activity was investigated for the study site and individual landslide as, in certain cases, a correlation between thaw depths and FDD could be found in other regions of Svalbard (Strand et al., 2021). A weak correlation between FDD and landslide activity during a year (R = 0.26) was found, and further shifts in the arctic maritime climate may change this as the FDD may also be considered a thermal reset between individual thaw periods. No trend for FDD could be identified between 2011 and 2021 (R = 0.02). The impact of FDD on the depth of thaw also depends on the thickness, duration and consistency of the snow cover (Strand et al., 2021). Climate change can be expected to further facilitate the observed landslide processes, given that temperature thresholds during either the thawing or freezing period are exceeded.

## 6. Conclusions

743

744

745

746

747

748

749

750

751

752

753

754

755

756

757

758

759

760

761

762

763

764

765

766

767

Landslide processes affecting steep sediment-mantled slopes in the studied Austre Lovénbreen basin are investigated based on several methods, consisting of (i) geomorphological mapping, (ii) multi-temporal TLS surveys, and (iii) visual monitoring via an automated camera network and subsequent image analysis. Multi-temporal TLS campaigns with a high spatial resolution allowed us to detect and quantify complex terrain changes between the TLS campaigns within the level of detection in the range of centimetres (LOD95%). The combined analysis of quantitative TLS data with qualitative data from the automated camera network allowed for investigating the impact of meteorological factors on landslide trigger mechanisms, kinematics and the evolution of paraglacial slopes following glacier retreat and downwastage. With increasing distance to the glacier terminus, a spatial and temporal variation of landslide processes from translational debris slides towards debris flows was observed, indicating a lateral succession of processes dominating the paraglacial evolution of the sediment-mantled slopes. Generally, landslide frequency and magnitude decreased with distance to the glacier. Landslide phenomena were the most dominant source of surface change, with respect to the retreat of the glacier itself, during the observation period. Translational debris slides accounted for 96% of paraglacial sediment transport affecting sediment-mantled slopes in the studied Austre Lovénbreen basin and are controlled by a combination of meteorological factors, foremost rainfall and temperature. The spatial distribution of an ice-layer within slopes serving as the rupture surface of observed translational debris slides and the thermal regime during a year are the main aspects enabling potential translational debris slides. However, heavy rainfall events within the hydrological summer are the main factor contributing to the magnitude and frequency of the slides. A weak correlation between debris flow activity and

increased rainfalls during the observation period could be found.

Finally, the increased landslide frequency and magnitude within the observation period showed the acceleration of climate-induced changes modifying the landscape within this high-Arctic environment. Our results show that the intensity of the thawing period and heavy rainfall events are crucial for paraglacial adjustment of steep sediment-mantled slopes. The expected continuous temperature rise and heavy rainfall events may further facilitate landslide processes in the Arctic.

We stress that long-term observatories, such as the Austre Lovénbreen glacier basin, are irreplaceable for future research focusing on glacial and paraglacial responses to climate change in the high-Arctic as the quantification of these processes may serve as additional climate change proxies to indicate past and present climate alterations and may provide insights also relevant for other regions as climate change is more pronounced at higher latitudes.

## **CRediT** authorship contribution statement

Erik Kuschel: Writing – Original draft, Investigation, Data Curation, Methodology, Formal analysis, Visualization, Conceptualization. Florian Tolle: Conceptualization, Investigation, Writing – Review & Editing, Supervision, Project administration, Funding acquisition. Ursula Laa: Formal analysis, Visualization. Vinzent Klaus: Writing - Review & Editing, Formal analysis. Alexander Prokop: Investigation, Data Curation. Jean-Michel Friedt: Software, Investigation, Data Curation. Eric Bernard: Investigation. Christian Zangerl: Writing – Review & Editing, Investigation, Supervision.

## **Declaration of competing interest**

The authors declare that they have no known competing financial interests or personal relationships that could have appeared to influence the work reported in this paper.

## Acknowledgements

This study is part of the PRISM project, supported by the French Polar Institute Paul-Émile Victor (IPEV), French Agence Nationale de la Recherche, Région Bourgogne Franche-Comté, and CNRS Groupement de Recherche Arctique. Open access funding is provided by BOKU University, Austria.

## 797 Literature:

798 Abellán, A., Oppikofer, T., Jaboyedoff, M., Rosser, N. J., Lim, M., & Lato, M. J. (2014). Terrestrial laser 799 scanning of rock slope instabilities. Earth Surface Processes and Landforms, 39(1). 800 https://doi.org/10.1002/esp.3493 801 Agliardi, F., Crosta, G., & Zanchi, A. (2001). Structural constraints on deep-seated slope deformation 802 kinematics. Engineering Geology, 59(1-2). https://doi.org/10.1016/S0013-7952(00)00066-1 803 Akerman, H. J. (1984). Notes on talus morphology and processes in Spitsbergen. Geografiska Annaler, 804 Series A, 66 A(4). https://doi.org/10.1080/04353676.1984.11880115 805 André, MF. (1986). Dating slope deposits and estimating rates of rock wall retreat in northwest 806 Spitsbergen by lichenometry. Geografiska Annaler, Series Α, 68 A(1-2). 807 https://doi.org/10.1080/04353676.1986.11880159 808 André, MF. (1990). Geomorphic impact of spring avalanches in Northwest Spitsbergen (79° N). 809 Permafrost and Periglacial Processes, 1(2). https://doi.org/10.1002/ppp.3430010203 810 André, MF. (1996). Geological control of slope processes in northwest Spitsbergen. Norsk Geografisk 811 Tidsskrift, 50(1). https://doi.org/10.1080/00291959608552350 812 Ballantyne, C. K. (2002). Paraglacial geomorphology. In Quaternary Science Reviews (Vol. 21). 813 Ballantyne, C. K., & Benn, D. I. (1994). Paraglacial slope adjustment and resedimentation following 814 recent glacier retreat, Fabergstolsdalen, Norway. Arctic & Alpine Research, 26(3). 815 https://doi.org/10.2307/1551938 816 Barbaroux, L. (1967). Le Quaternaire de la Péninsule de Broker et régions voisines (Spitsberg 817 occidental). Bulletin de l'Association Française Pour l'étude Du Quaternaire, 818 https://doi.org/10.3406/guate.1967.1068 819 Bergh, S. G., Maher, H. D., & Braathen, A. (2000). Tertiary divergent thrust directions from partitioned 820 transpression. Broggerhalvoya, Spitsbergen. Norsk Geologisk Tidsskrift, 80(2). 821 https://doi.org/10.1080/002919600750042573 822 Bernard, É., Friedt, J. M., Saintenoy, A., Tolle, F., Griselin, M., & Marlin, C. (2014). Where does a glacier 823 end? GPR measurements to identify the limits between valley slopes and actual glacier body. 824 Application to the Austre Lovénbreen, Spitsbergen. International Journal of Applied Earth 825 Observation and Geoinformation, 27(PARTA). https://doi.org/10.1016/j.jag.2013.07.006

826 Bernard, É., Friedt, J. M., Tolle, F., Griselin, M., Martin, G., Laffly, D., & Marlin, C. (2013). Monitoring 827 seasonal snow dynamics using ground based high resolution photography (Austre Lovénbreen, 828 Svalbard, 79°N). ISPRS Journal of Photogrammetry and Remote Sensing, 75. 829 https://doi.org/10.1016/j.isprsjprs.2012.11.001 830 Berthling, I., & Etzelmüller, B. (2007). Holocene rockwall retreat and the estimation of rock glacier age, 831 Prins Karls Forland, Svalbard. Geografiska Annaler, Series A: Physical Geography, 89(1). 832 https://doi.org/10.1111/j.1468-0459.2007.00309.x 833 Besl, P. J., & McKay, N. D. (1992). A Method for Registration of 3-D Shapes. IEEE Transactions on 834 Pattern Analysis and Machine Intelligence, 14(2). https://doi.org/10.1109/34.121791 835 Błaszczyk, M., Jania, J. A., & Hagen, J. O. (2009). Tidewater glaciers of Svalbard: Recent changes and 836 estimates of calving fluxes. Polish Polar Research, 30(2). 837 Chen, Y., & Medioni, G. (1991). Object modeling by registration of multiple range images. *Proceedings* 838 IEEE International Conference on Robotics and Automation, 3. 839 https://doi.org/10.1109/robot.1991.132043 840 Chiarle, M., Iannotti, S., Mortara, G., & Deline, P. (2007). Recent debris flow occurrences associated 841 with glaciers in the Alps. Global and Planetary Change, *56*(1–2). 842 https://doi.org/10.1016/j.gloplacha.2006.07.003 843 Christiansen, H., Humlum, O., & Eckerstorfer, M. (2013). Central svalbard 2000-2011 meteorological 844 dynamics and periglacial landscape response. Arctic, Antarctic, and Alpine Research, 45(1). 845 https://doi.org/10.1657/1938-4246-45.16 846 Church, M., & Ryder, J. M. (1972). Paraglacial sedimentation: A consideration of fluvial processes 847 conditioned by glaciation. Bulletin of the Geological Society of America, 83(10). 848 https://doi.org/10.1130/0016-7606(1972)83[3059:PSACOF]2.0.CO;2 849 CloudCompare. (2021). CloudCompare Version 2.13. Retrieved from http://www.cloudcompare.org/. 850 Crosta, G. B., Frattini, P., & Agliardi, F. (2013). Deep seated gravitational slope deformations in the 851 European Alps. In Tectonophysics (Vol. 605). https://doi.org/10.1016/j.tecto.2013.04.028 852 Crozier, M. J. (2010). Deciphering the effect of climate change on landslide activity: A review. In

Geomorphology (Vol. 124, Issues 3-4). https://doi.org/10.1016/j.geomorph.2010.04.009

854 Cruden, D. M. (1991). A simple definition of a landslide. Bulletin of the International Association of 855 Engineering Geology - Bulletin de l'Association Internationale de Géologie de l'Ingénieur, 43(1). 856 https://doi.org/10.1007/BF02590167 857 Cruden, D. M., & Hu, X. Q. (1993). Exhaustion and steady state models for predicting landslide hazards 858 in the Canadian Rocky Mountains. Geomorphology, 8(4). https://doi.org/10.1016/0169-859 555X(93)90024-V 860 Cruden, D. M., & Varnes, D. J. (1996). Landslide types and processes. Special Report - National 861 Research Council, Transportation Research Board, 247. 862 Curry, A. M. (1999). Paraglacial modification of slope form. Earth Surface Processes and Landforms, 863 24(13). https://doi.org/10.1002/(SICI)1096-9837(199912)24:13<1213::AID-ESP32>3.0.CO;2-B 864 De Haas, T., Kleinhans, M. G., Carbonneau, P. E., Rubensdotter, L., & Hauber, E. (2015). Surface 865 morphology of fans in the high-Arctic periglacial environment of Svalbard: Controls and processes. 866 Earth-Science Reviews, 146, 163-182. https://doi.org/10.1016/J.EARSCIREV.2015.04.004 867 Dhakal, A. S., & Sidle, R. C. (2004). Distributed simulations of landslides for different rainfall conditions. 868 Hydrological Processes, 18(4). https://doi.org/10.1002/hyp.1365 869 Eckerstorfer, M., & Christiansen, H. (2011). The "high arctic maritime snow climate" in Central svalbard. 870 Arctic, Antarctic, and Alpine Research, 43(1), https://doi.org/10.1657/1938-4246-43.1.11 871 Evans, S. G., & Claque, J. J. (1994). Recent climatic change and catastrophic geomorphic processes 872 mountain environments. Geomorphology, *10*(1–4). https://doi.org/10.1016/0169in 873 555X(94)90011-6 874 Fahnestock, M. A., Scambos, T. A., & Bindschadler, R. A. (1992). Semi-automated ice velocity 875 determination from satellite imagery. Eos, 73(493). 876 Farnsworth, W. R., Allaart, L., Ingólfsson, Ó., Alexanderson, H., Forwick, M., Noormets, R., Retelle, M., 877 & Schomacker, A. (2020). Holocene glacial history of Svalbard: Status, perspectives and 878 challenges. In Earth-Science Reviews (Vol. 208). https://doi.org/10.1016/j.earscirev.2020.103249 879 Fey, C., & Wichmann, V. (2017). Long-range terrestrial laser scanning for geomorphological change 088 detection in alpine terrain - handling uncertainties. Earth Surface Processes and Landforms,

42(5). https://doi.org/10.1002/esp.4022

882	Fitzsimons, S. J. (1996). Paraglacial redistribution of glacial sediments in the Vestfold Hills, East							
883	Antarctica. Geomorphology, 15(2). https://doi.org/10.1016/0169-555X(95)00122-L							
884	Francis, J. A., Vavrus, S. J., & Cohen, J. (2017). Amplified Arctic warming and mid-latitude weather:							
885	new perspectives on emerging connections. Wiley Interdisciplinary Reviews: Climate Change,							
886	8(5). https://doi.org/10.1002/wcc.474							
887	French, H. M. (2013). The periglacial environment: Third edition. In <i>The Periglacial Environment: Third</i>							
888	Edition. https://doi.org/10.1002/9781118684931							
889	Friedt, J. M., Bernard, É., & Griselin, M. (2023). Ground-Based Oblique-View Photogrammetry and							
890	Sentinel-1 Spaceborne RADAR Reflectivity Snow Melt Processes Assessment on an Arctic							
891	Glacier. Remote Sensing, 15(7). https://doi.org/10.3390/rs15071858							
892	Friedt, J. M., Tolle, F., Bernard, É., Griselin, M., Laffly, D., & Marlin, C. (2012). Assessing the relevance							
893	of digital elevation models to evaluate glacier mass balance: Application to Austre Lovénbreen							
894	(Spitsbergen, 79°N). Polar Record, 48(1). https://doi.org/10.1017/S0032247411000465							
895	Gariano, S. L., & Guzzetti, F. (2016). Landslides in a changing climate. In Earth-Science Reviews (Vol.							
896	162, pp. 227–252). Elsevier B.V. https://doi.org/10.1016/j.earscirev.2016.08.011							
897	Girod, L., Ivar Nielsen, N., Couderette, F., Nuth, C., & Kääb, A. (2018). Precise DEM extraction from							
898	Svalbard using 1936 high oblique imagery. Geoscientific Instrumentation, Methods and Data							
899	Systems, 7(4). https://doi.org/10.5194/gi-7-277-2018							
900	Hagen, J. O., Kohler, J., Melvold, K., & Winther, J. G. (2003). Glaciers in Svalbard: Mass balance, runoff							
901	and freshwater flux. Polar Research, 22(2). https://doi.org/10.1111/j.1751-8369.2003.tb00104.x							
902	Harris, C., Arenson, L. U., Christiansen, H. H., Etzelmüller, B., Frauenfelder, R., Gruber, S., Haeberli,							
903	W., Hauck, C., Hölzle, M., Humlum, O., Isaksen, K., Kääb, A., Kern-Lütschg, M. A., Lehning, M.,							
904	Matsuoka, N., Murton, J. B., Nötzli, J., Phillips, M., Ross, N., Vonder Mühll, D. (2009).							
905	Permafrost and climate in Europe: Monitoring and modelling thermal, geomorphological and							
906	geotechnical responses. In Earth-Science Reviews (Vol. 92, Issues 3-4).							
907	https://doi.org/10.1016/j.earscirev.2008.12.002							
908	Hinkel, K. M., & Nicholas, J. R. (1995). Active layer thaw rate at a boreal forest site in central Alaska,							
909	USA. Arctic and Alpine Research, 27(1). https://doi.org/10.2307/1552069							

- Hjelle A. Q. Y, Piepjohn K, Saalmann K, Salvigsen O, Thiedig F, & Dallmann K. (1999). Geological map
  of Svalbard 1:100 000, sheet A7G Kongsfjorden. *Norsk Polarinstitutt Temakart No. 22, 56 Pp.*
- 912 Hübl, J. (2018). Conceptual framework for sediment management in torrents. Water (Switzerland),
- 913 *10*(12). https://doi.org/10.3390/w10121718
- 914 Huggel, C., Clague, J. J., & Korup, O. (2012). Is climate change responsible for changing landslide
- 915 activity in high mountains? Earth Surface Processes and Landforms, 37(1).
- 916 https://doi.org/10.1002/esp.2223
- 917 Humlum, O., Elberling, B., Hormes, A., Fjordheim, K., Hansen, O. H., & Heinemeier, J. (2005). Late-
- Holocene glacier growth in Svalbard, documented by subglacial relict vegetation and living soil
- 919 microbes. *Holocene*, *15*(3). https://doi.org/10.1191/0959683605hl817rp
- Hungr, O., Leroueil, S., & Picarelli, L. (2014). The Varnes classification of landslide types, an update.
- 921 In Landslides (Vol. 11, Issue 2). https://doi.org/10.1007/s10346-013-0436-y
- Hürlimann, M., Coviello, V., Bel, C., Guo, X., Berti, M., Graf, C., Hübl, J., Miyata, S., Smith, J. B., & Yin,
- 923 H. Y. (2019). Debris-flow monitoring and warning: Review and examples. In *Earth-Science*
- 924 Reviews (Vol. 199). https://doi.org/10.1016/j.earscirev.2019.102981
- 925 IPCC. (2014). Climate Change 2014: Synthesis Report. Contribution of Working Groups I, II and III to
- the Fifth Assessment Report of the Intergovernmental Panel on Climate Change. In *Ipcc*.
- 927 IPCC. (2021). Climate Change 2021: The Physical Science Basis. Working Group I Contribution to the
- 928 IPCC Sixth Assessment Report. Climate Change 2021: The Physical Science Basis.
- 929 Irvine-Fynn, T. D. L., Hodson, A. J., Moorman, B. J., Vatne, G., & Hubbard, A. L. (2011). Polythermal
- glacier hydrology: A review. In Reviews of Geophysics (Vol. 49, Issue 4).
- 931 https://doi.org/10.1029/2010RG000350
- Jahn, A. (1967). Some Features of Mass Movement on Spitsbergen Slopes. In Source: Geografiska
- 933 Annaler. Series A, Physical Geography (Vol. 49, Issue 4).
- Lague, D., Brodu, N., & Leroux, J. (2013). Accurate 3D comparison of complex topography with
- 935 terrestrial laser scanner: Application to the Rangitikei canyon (N-Z). ISPRS Journal of
- 936 Photogrammetry and Remote Sensing, 82. https://doi.org/10.1016/j.isprsjprs.2013.04.009

937	Lewkowicz, A. G., & Harris, C. (2005). Frequency and magnitude of active-layer detachment failures in							
938	discontinuous and continuous permafrost, northern Canada. Permafrost and Periglacia							
939	Processes, 16(1). https://doi.org/10.1002/ppp.522							
940	Macfarlane, D. F. (2009). Observations and predictions of the behaviour of large, slow-moving							
941	landslides in schist, Clyde Dam reservoir, New Zealand. Engineering Geology, 109(1-2).							
942	https://doi.org/10.1016/j.enggeo.2009.02.005							
943	Marlin, C., Tolle, F., Griselin, M., Bernard, E., Saintenoy, A., Quenet, M., & Friedt, J. M. (2017). Change							
944	in geometry of a high arctic glacier from 1948 to 2013 (Austre Lovénbreen, Svalbard). Geografiska							
945	Annaler, Series A: Physical Geography, 99(2). https://doi.org/10.1080/04353676.2017.1285203							
946	Martín-Moreno, R., & Allende-Álvarez, F. (2016). Little Ice Age glacier extension and retreat in							
947	Spitsbergen Island (High Arctic, Svalbard Archipelago). Cuadernos de Investigación Geográfica,							
948	42(2). https://doi.org/10.18172/cig.2919							
949	Matsuoka, N. (1991). A model of the rate of frost shattering: Application to field data from Japan,							
950	Svalbard and Antarctica. Permafrost and Periglacial Processes, 2(4).							
951	https://doi.org/10.1002/ppp.3430020403							
952	Matthews, J. A., Winkler, S., Wilson, P., Tomkins, M. D., Dortch, J. M., Mourne, R. W., Hill, J. L., Owen,							
953	G., & Vater, A. E. (2018). Small rock-slope failures conditioned by Holocene permafrost							
954	degradation: a new approach and conceptual model based on Schmidt-hammer exposure-age							
955	dating, Jotunheimen, southern Norway. Boreas, 47(4). https://doi.org/10.1111/bor.12336							
956	Mattson, L. E., & Gardner, J. S. (1991). Mass wasting on valley-side ice-cored moraines, Boundary							
957	Glacier, Alberta, Canada. Geografiska Annaler, Series A, 73 A(3-4).							
958	https://doi.org/10.1080/04353676.1991.11880337							
959	Maturilli, M., Hanssen-Bauer, I., Neuber, R., Rex, M., & Edvardsen, K. (2019). The Atmosphere Above							
960	Ny-Ålesund: Climate and Global Warming, Ozone and Surface UV Radiation.							
961	https://doi.org/10.1007/978-3-319-46425-1_2							
962	Mercier, D., Étienne, S., Sellier, D., & André, M. F. (2009). Paraglacial gullying of sediment-mantled							
963	slopes: A case study of Colletthøgda, Kongsfjorden area, West Spitsbergen (Svalbard). Earth							
964	Surface Processes and Landforms 34(13) 1772–1789 https://doi.org/10.1002/esp.1862							

- 965 MET Norway. (2021). Norwegian Meteorological Institut (https://www.met.no/en). Norwegian
- Meteorological Institut. https://www.met.no/
- 967 Mittelholzer W. (1923). Kingsbai mit Kingsgletscher und Lovenfirnen von Osten aus 1700 m Höhe-
- 968 Spitzbergenflug 1923. In ETH-Bibliothek\_LBS\_MH02-01-0041;
- https://commons.wikimedia.org/wiki/Category:ETH-BIB\_Mittelholzer-Spitsbergen\_flight\_1923.
- 970 Mountains, S., Rapp, A., & Strömquist, L. (1976). Slope Erosion due to Extreme Rainfall in the. In
- 971 Source: Geografiska Annaler. Series A, Physical Geography (Vol. 58, Issue 3).
- 972 Nordli, Ø., Przybylak, R., Ogilvie, A. E. J., & Isaksen, K. (2014). Long-term temperature trends and
- 973 variability on spitsbergen: The extended svalbard airport temperature series, 1898-2012. *Polar*
- 974 Research, 33(1 SUPPL). https://doi.org/10.3402/polar.v33.21349
- 975 NPI. (2014). Terrengmodell Svalbard (S0 Terrengmodell) [Data set]. Norwegian Polar Institute.
- 976 Https://Doi.Org/10.21334/Npolar.2014.Dce53a47.
- 977 Owen, L. A. (1991). Mass movement deposits in the Karakoram Mountains: their sedimentary
- characteristics, recognition and role in Karakoram landform evolution.
- 979 Patton, A. I., Rathburn, S. L., & Capps, D. M. (2019). Landslide response to climate change in
- 980 permafrost regions. In Geomorphology (Vol. 340).
- 981 https://doi.org/10.1016/j.geomorph.2019.04.029
- Pepin, N., Bradley, R. S., Diaz, H. F., Baraer, M., Caceres, E. B., Forsythe, N., Fowler, H., Greenwood,
- G., Hashmi, M. Z., Liu, X. D., Miller, J. R., Ning, L., Ohmura, A., Palazzi, E., Rangwala, I., Schöner,
- W., Severskiy, I., Shahgedanova, M., Wang, M. B., ... Yang, D. Q. (2015). Elevation-dependent
- warming in mountain regions of the world. In *Nature Climate Change* (Vol. 5, Issue 5, pp. 424–
- 986 430). Nature Publishing Group. https://doi.org/10.1038/nclimate2563
- Peruccacci, S., Brunetti, M. T., Gariano, S. L., Melillo, M., Rossi, M., & Guzzetti, F. (2017). Rainfall
- 988 thresholds for possible landslide occurrence in Italy. Geomorphology, 290.
- 989 https://doi.org/10.1016/j.geomorph.2017.03.031
- 990 Prokop, A. (2008). Assessing the applicability of terrestrial laser scanning for spatial snow depth
- 991 measurements. Cold Regions Science and Technology, 54(3).
- 992 https://doi.org/10.1016/j.coldregions.2008.07.002

993 Prokop, A., & Panholzer, H. (2009). Assessing the capability of terrestrial laser scanning for monitoring 994 slow moving landslides. Natural Hazards and Earth System Science. 9(6). 995 https://doi.org/10.5194/nhess-9-1921-2009 996 Rapp, A. (1960). Talus slopes and mountain walls at Tempelfjorden, Spitsbergen: a geomorphological 997 study of the denudation of slopes in an arctic locality. 998 Rechberger, C., Fey, C., & Zangerl, C. (2021). Structural characterisation, internal deformation, and 999 kinematics of an active deep-seated rock slide in a valley glacier retreat area. Engineering 1000 Geology, 286. https://doi.org/10.1016/j.enggeo.2021.106048 1001 RIEGL. (2010a). Data Sheet: Riegl LMS-420i Long Range & High Accuracy 3D Terrestrial Laser 1002 Scanner. 1003 RIEGL. (2010b). Data Sheet: Riegl LPM-321 Long Range Laser Profile Measurement System. RIEGL 1004 Laser Measurement Systems. 1005 RIEGL. (2013). Operating and Processing Software RiScan Pro for RIEGL 3D Laser scanners. RIEGL 1006 LMS GmbH. 1007 RIEGL. (2016). Data Sheet: Riegl VZ-6000 - 3D Ultra long range terrestrial laserscanner with online 1008 waveform processing. RIEGL Laser Measurement Systems. 1009 Saalmann, K., & Thiedig, F. (2001). Tertiary West Spitsbergen fold and thrust belt on brøggerhalvøya, 1010 Svalbard: Structural evolution and kinematics. Tectonics. 20(6). 1011 https://doi.org/10.1029/2001TC900016 1012 Saalmann, K., & Thiedig, F. (2002). Thrust tectonics on Brøggerhalvøya and their relationship to the 1013 Tertiary West Spitsbergen fold-and-thrust belt. Geological Magazine, 139(1), 47-72. 1014 https://doi.org/10.1017/S0016756801006069 1015 Scambos, T. A., Dutkiewicz, M. J., Wilson, J. C., & Bindschadler, R. A. (1992). Application of image 1016 cross-correlation to the measurement of glacier velocity using satellite image data. Remote 1017 Sensing of Environment, 42(3). https://doi.org/10.1016/0034-4257(92)90101-O 1018 Schaefer, K., Zhang, T., Bruhwiler, L., & Barrett, A. P. (2011). Amount and timing of permafrost carbon 1019 release in response to climate warming. Tellus, Series B: Chemical and Physical Meteorology,

63(2). https://doi.org/10.1111/j.1600-0889.2011.00527.x

1021 Seneviratne, S. I., Nicholls, N., Easterling, D., Goodess, C. M., Kanae, S., Kossin, J., Luo, Y., Marengo, 1022 J., Mc Innes, K., Rahimi, M., Reichstein, M., Sorteberg, A., Vera, C., Zhang, X., Rusticucci, M., 1023 Semenov, V., Alexander, L. V., Allen, S., Benito, G., ... Zwiers, F. W. (2012). Changes in climate 1024 extremes and their impacts on the natural physical environment. In Managing the Risks of Extreme 1025 Events and Disasters to Advance Climate Change Adaptation: Special Report of the 1026 Intergovernmental (Vol. 9781107025066). Panel on Climate Change 1027 https://doi.org/10.1017/CBO9781139177245.006 1028 Siewert, M. B., Krautblatter, M., Christiansen, H. H., & Eckerstorfer, M. (2012). Arctic rockwall retreat 1029 rates estimated using laboratory-calibrated ERT measurements of talus cones in Longyeardalen, 1030 Svalbard. Earth Surface Processes and Landforms, 37(14). https://doi.org/10.1002/esp.3297 1031 Snyder, J. A., Werner, A., & Miller, G. H. (2000). Holocene cirque glacier activity in western Spitsbergen, 1032 Svalbard: Sediment records from proglacial Linnevatnet. Holocene, 10(5). 1033 https://doi.org/10.1191/095968300667351697 1034 Soldati, M., Corsini, A., & Pasuto, A. (2004). Landslides and climate change in the Italian Dolomites 1035 since the Late glacial. Catena, 55(2). https://doi.org/10.1016/S0341-8162(03)00113-9 1036 Stefan, J. (1890). Probleme der Theorie der Warmeleitung. Sitzungsberichte Der Mathematisch-1037 Naturwissenschaftlichen Classe Der Kaiserlichen Akademie Der Wissenschaften. 1038 Stiny J. (1910). Die Muren: Versuch einer Monographie mit besonderer berücksichtigung der 1039 verhältnisse in Den Tiroler Alpen. Wagner. 1040 Strand, S. M., Christiansen, H. H., Johansson, M., Åkerman, J., & Humlum, O. (2021). Active layer 1041 thickening and controls on interannual variability in the Nordic Arctic compared to the circum-1042 Arctic. Permafrost and Periglacial Processes, 32(1). https://doi.org/10.1002/ppp.2088 1043 Svendsen, J. I., & Mangerud, J. (1997). Holocene glacial and climatic variations on Spitsbergen, 1044 Svalbard. Holocene, 7(1). https://doi.org/10.1177/095968369700700105 1045 Tarini, M., Cignoni, P., & Montani, C. (2006). Ambient occlusion and edge cueing to enhance real time 1046 molecular visualization. IEEE Transactions on Visualization and Computer Graphics, 12(5).

https://doi.org/10.1109/TVCG.2006.115

1048	Telling, J., Lyda, A., Hartzell, P., & Glennie, C. (2017). Review of Earth science research using terrestrial								
1049	laser	scanning.	ln	Earth-Science	Reviews	(Vol.	169).		
1050	https://doi.org/10.1016/j.earscirev.2017.04.007								
1051	Terzaghi, K. (1950). <i>Mechanism of landslides</i> .								
1052	Tolgensbakk J, & Sollid JL. (1980). Kvadehuksletta, geomorfologi og kvartærgeologi 1:10,000								
1053	(Kvadehuksletta, geomorphology and Quaternary geology 1:10,000.). In Dept. of Physica								
1054	Geography, University of Oslo.								
1055	Wheaton, J. M., Brasington, J., Darby, S. E., & Sear, D. A. (2010). Accounting for uncertainty in DEMs								
1056	from repeat topographic surveys: Improved sediment budgets. Earth Surface Processes and								
1057	Landforms, 35(2). https://doi.org/10.1002/esp.1886								
1058	Zangerl, C., Eberhardt, E., & Perzlmaier, S. (2010). Kinematic behaviour and velocity characteristics of								
1059	a complex deep-seated crystalline rockslide system in relation to its interaction with a dam								
1060	reservoir. Engineering Geology, 112(1-4). https://doi.org/10.1016/j.enggeo.2010.01.001								
1061	Zangerl, C.,	Prager, C., Bra	andner, R	, & Brückl, E. (	2008). Methodis	scher Leitfad	en zur		
1062	prozessorientierten Bearbeitung von Massenbewegungen. Geo. Alp, 5.								
1063	Zhang, T., & St	amnes, K. (1998).	Impact of	climatic factors on the	active layer and	permafrost at	Barrow,		
1064	Alaska.	Permafrost and	Periglad	cial Processes, 9(3	3). https://doi.or	rg/10.1002/(sid	ci)1099-		
1065	1530(199807/09)9:3<229::aid-ppp286>3.0.co;2-t								
1066	Zimmermann, M., & Haeberli, W. (1992). Climatic change and debris flow activity in high-mountain								
1067	areas - a case study in the Swiss Alps. Catena Supplement, 22.								